REPORT DOCUMENTATION PAGE

1. REPORT DATE (DD-MM-YYYY)	2. REPORT TYPE	3. DATES COVERED (From - To)
03-06-2008	Journal Article	

4. TITLE AND SUBTITLE

On the Relationship Between Satellite-estimated Bio-optical and Thermal Properties in the Gulf of Mexico

5a. CONTRACT NUMBER

5b. GRANT NUMBER

5c. PROGRAM ELEMENT NUMBER
0601153N

6. AUTHOR(S)

Jason Jolliff, John C. Kindle, Bradley Penta, Robert Helber, Zhongping Lee, Igor G. Shulman, Robert A. Arnone, Clark D. Rowley

5d. PROJECT NUMBER

5e. TASK NUMBER

5f. WORK UNIT NUMBER
73-8404-06-5

7. PERFORMING ORGANIZATION NAME(S) AND ADDRESS(ES)

Naval Research Laboratory
Oceanography Division
Stennis Space Center, MS 39529-5004

8. PERFORMING ORGANIZATION REPORT NUMBER
NRL/JA/7330-06-6303

9. SPONSORING/MONITORING AGENCY NAME(S) AND ADDRESS(ES)

Office of Naval Research
800 N. Quincy St.
Arlington, VA 22217-5660

10. SPONSOR/MONITOR'S ACRONYM(S)
ONR

11. SPONSOR/MONITOR'S REPORT NUMBER(S)

12. DISTRIBUTION/AVAILABILITY STATEMENT

Approved for public release, distribution is unlimited.

13. SUPPLEMENTARY NOTES

20080610 103

14. ABSTRACT

Three years of Sea-viewing Wide Field-of-view Sensor (SeaWiFS) ocean color data were combined with three-dimensional thermal fields generated by the U.S. Navy's Modular Ocean Data Assimilation System (MODAS) in order to examine the interdependencies between bio-optical fields and their relationship to seasonal and mesoscale changes in upper ocean thermal structure. The combined data set suggests that the oceanic boundary layer within the Gulf of Mexico may be broadly defined by two seasonally occurring bio-thermal periods. A winter mixing period, characterized by net heat losses to the atmosphere, deepening of the isothermal layer depth, and annual maxima of satellite-estimated colored detrital matter (CDM) absorption coefficients and surface pigment concentration, was followed by a thermally stratified period characterized by net surface ocean heating, reduced isothermal layer depths, and annual minima in surface bio-optical fields. Variability in the interdependencies of ocean color products was used to diagnose an attendant shift in the size-structure of surface phytoplankton communities as well as identify CDM as the constituent responsible for the majority of blue-light absorption in Gulf of Mexico surface waters. The mesoscale circulation, as resolved by MODAS thermal fields into cold and warm-core eddies, appears to significantly modulate the seasonal bio-optical cycle of CDM absorption and surface pigment concentration. An empirical model was developed to describe CDM absorption as a function of upper ocean thermal energy. The model accounted for nearly half ...

15. SUBJECT TERMS

ocean color, color dissolved organic matter, phytoplankton absorption, biophysical processes

16. SECURITY CLASSIFICATION OF:			17. LIMITATION OF ABSTRACT	18. NUMBER OF PAGES	19a. NAME OF RESPONSIBLE PERSON
a. REPORT	b. ABSTRACT	c. THIS PAGE			Jason Jolliff
Unclassified	Unclassified	Unclassified	UL	27	19b. TELEPHONE NUMBER (Include area code) 228-688-5308

Click
Here
for
**Full
Article**

On the relationship between satellite-estimated bio-optical and thermal properties in the Gulf of Mexico

Jason K. Jolliff,[1] John C. Kindle,[1] Bradley Penta,[1] Robert Helber,[1] Zhongping Lee,[1] Igor Shulman,[1] Robert Arnone,[1] and Clark D. Rowley[1]

[1] Three years of Sea-viewing Wide Field-of-view Sensor (SeaWiFS) ocean color data were combined with three-dimensional thermal fields generated by the U.S. Navy's Modular Ocean Data Assimilation System (MODAS) in order to examine the interdependencies between bio-optical fields and their relationship to seasonal and mesoscale changes in upper ocean thermal structure. The combined data set suggests that the oceanic boundary layer within the Gulf of Mexico may be broadly defined by two seasonally occurring bio-thermal periods. A winter mixing period, characterized by net heat losses to the atmosphere, deepening of the isothermal layer depth, and annual maxima of satellite-estimated colored detrital matter (CDM) absorption coefficients and surface pigment concentration, was followed by a thermally stratified period characterized by net surface ocean heating, reduced isothermal layer depths, and annual minima in surface bio-optical fields. Variability in the interdependencies of ocean color products was used to diagnose an attendant shift in the size-structure of surface phytoplankton communities as well as identify CDM as the constituent responsible for the majority of blue-light absorption in Gulf of Mexico surface waters. The mesoscale circulation, as resolved by MODAS thermal fields into cold and warm-core eddies, appears to significantly modulate the seasonal bio-optical cycle of CDM absorption and surface pigment concentration. An empirical model was developed to describe CDM absorption as a function of upper ocean thermal energy. The model accounted for nearly half the variance in the satellite-estimate of this bio-optical variable. Large mismatches between the model and satellite data implied episodes of shelf water export to the deep Gulf of Mexico.

1. Introduction

[2] The mechanism of the spring phytoplankton bloom in temperate waters has long been the canonical example of coupled biological and physical processes in the upper ocean [*Sverdrup*, 1953]. Its core conceptual facet is that dynamic gain and loss processes of the surface flora are indelibly linked to the density structure of the upper ocean such that vernal warming, and hence increasing thermal stratification, results in an optimal light and nutrient regime for phytoplankton growth, i.e., the critical depth theory [*Sverdrup*, 1953; *Mann and Lazier*, 1996; *Siegel et al.*, 2002a]. Biogeochemical element cycling in the surface ocean is in large part constrained by phytoplankton processes [e.g., *Falkowski*, 1994]. Phytoplankton biomass, in turn, is ostensibly constrained, in part, by the seasonal change in upper ocean thermal structure. Hence critical

depth theory implies a link between the ocean to atmosphere exchange of heat energy and the regulatory features of the biosphere, such as the sequestration of atmospheric carbon dioxide. In a broad sense, the potential coupling of surface ocean thermal energy variability to biogeochemical processes mediated by surface phytoplankton may be conceptually summarized with the term bio-thermal. Understanding the spatiotemporal variability of bio-thermal processes may be critical to ascertaining how future changes in the Earth's climate system may impact the biogeochemistry of the surface ocean.

[3] The synoptic scale and abundance of remote sensing data sets, which may provide estimates of both surface phytoplankton abundance and sea surface temperature (SST), make them ideally suited to study potential bio-thermal patterns within the ocean basins [e.g., *Obata et al.*, 1996; *Bricaud et al.*, 2002; *Espinosa-Carreon et al.*, 2004; *Uz and Yoder*, 2004; *Wilson and Coles*, 2005]. Nevertheless, there are two key obstacles to such a bio-thermal analysis that arise from the nature of these satellite data. First, satellite ocean color data are merely measurements of the

---

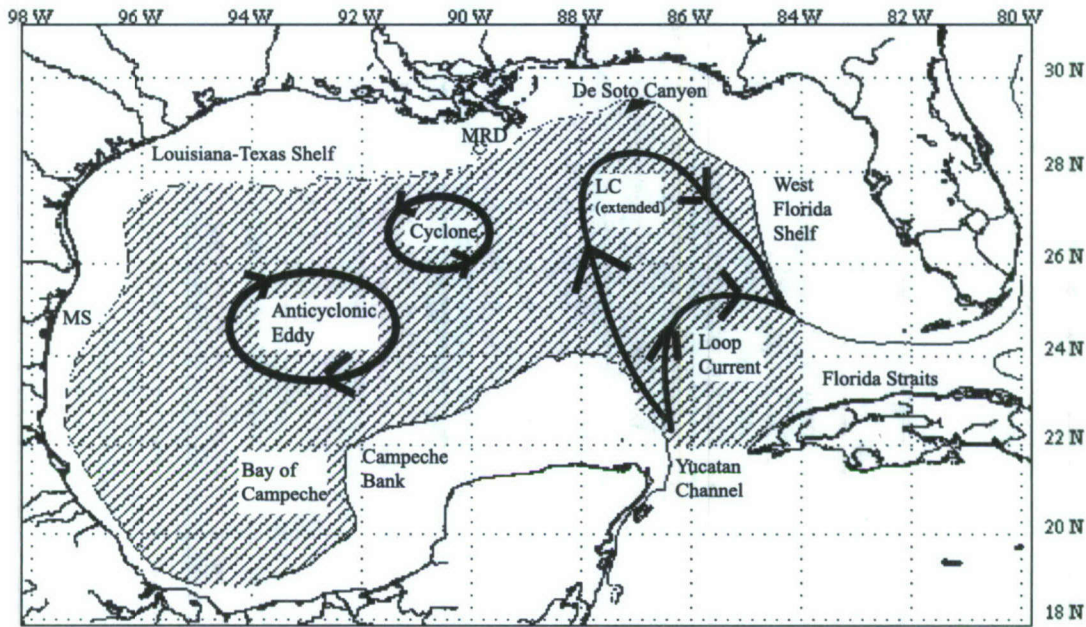[1]Naval Research Laboratory, Stennis Space Center, Mississippi, USA.

Figure 1. Map of the study area, the hatched region indicates the Gulf of Mexico deeper than 300 m. MRD, Mississippi River Delta; MS, Mexican Shelf. The deep Gulf of Mexico is partitioned from the Yucatan Channel by 22°N latitude and is further partitioned form the Florida Straits by 84°W longitude. The Loop Current (LC) is indicated for shortened and extended modes.

sea surface spectral reflectance, assuming the intervening atmosphere has been reasonably accounted for, and are not direct measurements of the standard proxy for phytoplankton biomass, surface chlorophyll-*a*, nor any other biological or bio-optical variable. Spectral reflectance is impacted by the angular structure of the light field as well as the optical properties of dissolved and particulate materials within the upper ∼30-m of the water column, which may consist of significant quantities of nonliving organic matter [*Carder et al.*, 1989, 1991; *Hochman et al.*, 1995]. Second, determination of SST from space-borne radiometer data is an indicator of the thermal energy in only the first few centimeters of the surface ocean [*Schluessel et al.*, 1987; *Hepplewhite*, 1989], and thus cannot directly yield information about the subsurface temperature structure.

[4] Recent advances in the way satellite data are used, however, have begun to address these deficiencies. Here we make service of recently developed ocean color algorithms that provide estimates of constituent absorption coefficients, which allow us to potentially assess the role of nonliving organic matter within ocean color variability and contrast the optical influence of these materials against that of surface phytoplankton. In addition, estimates of the three-dimensional temperature field are now routinely made by combining satellite SST, satellite altimetry data, and subsurface climatology [*Fox et al.*, 2002a]. These three-dimensional temperature fields allow us to examine dynamic changes in upper ocean thermal structure that were previously inaccessible to investigators relying solely upon the subsurface climatology. It is the goal of this paper to combine these advances in the way satellite data

are used to improve our understanding of bio-thermal patterns within the ocean basins.

2. Site Description

[5] Here we combine satellite-based estimates of three-dimensional thermal fields and surface bio-optical properties into a regional bio-thermal analysis for the Gulf of Mexico, a subtropical, semi-enclosed ocean basin (Figure 1). Previous studies of the satellite-estimated surface chlorophyll concentration within this basin have identified a seasonal cycle of winter chlorophyll maxima followed by summer minima [*Muller-Karger et al.*, 1991; *Biggs and Muller-Karger*, 1994]. This bio-optical pattern appears to be contemporaneous with the annual changes in the basin-averaged ocean-atmosphere heat energy exchange [*Virmani and Weisberg*, 2003], which presumably drive the seasonal cycle of convective winter overturn followed by thermally stratified summer conditions. Based on a combination of remote sensing observations, subsurface climatology, and ecosystem modeling [*Walsh et al.*, 1989; *Muller-Karger et al.*, 1991], seasonal changes in the depth of the surface mixed layer were hypothesized to be a determining constraint on phytoplankton biomass and productivity for this basin.

[6] Nevertheless, daily to monthly variability of upper ocean thermal structure in the Gulf of Mexico, hereafter referred to as the Gulf, is significantly impacted by the mesoscale circulation, which in turn, is dominated by the Loop Current and the associated eddy field. The Loop Current is effectively a large, anticyclonic feature that may extend as far north as ∼28°N or remain south of ∼24°N (Figure 1) as it leaves the Yucatan Channel and

transits the Gulf en route to the Florida Straits [*Maul*, 1977; *Maul and Vukovich*, 1993]. The Loop Current may intermittently spawn anticyclonic eddies 200–300 km in diameter that propagate towards the western Gulf [*Elliot*, 1982; *Vukovich and Crissman*, 1986; *Vukovich*, 1995; *Sturges and Leben*, 2000], and smaller (<200 km diameter) anticyclonic circulation features have also been observed [*Leben and Born*, 1993; *Vukovich*, 1995]. A diverse array of cyclonic circulation features is also typically present in the Gulf, often appearing where anticyclones interact with the continental shelf/slope or with one another [*Lewis and Kirwan*, 1985]. All of these circulation features modulate the depths of isotherms within the upper ~300-m of the water column [*Morrison and Nowlin*, 1976], and also appear to impact surface chlorophyll fields. The Loop Current and large eddy structures are discernable within ocean color imagery [*Maul and Gordon*, 1975; *Muller-Karger et al.*, 1991; *Biggs and Muller-Karger*, 1994; *Chassignet et al.*, 2005].

[7] Thus there are, at minimum, two salient scales of thermal and bio-optical variability in the Gulf: the seasonal cycle, the impact of which is generally synchronous throughout the basin [*Muller-Karger et al.*, 1991], and the mesoscale variability that arises as a result of the circulation. Superimposed upon these scales is the potential influence of low-salinity effluent. The most notable contributor is the Mississippi River, which has the sixth largest river discharge volume in the world [*Milliman and Meade*, 1983]. While river and estuarine effluent have notable influence upon coastal ocean color imagery in the Gulf [e.g., *Del Castillo et al.*, 2001; *Gilbes et al.*, 2002], our hypothesis is that their episodic influence upon the deep Gulf basin (>300-m depth; Figure 1) may be isolated within the satellite record once the seasonal to mesoscale patterns of bio-thermal variability have been quantified. Accordingly, section 4.1 examines the basin-wide average thermal and bio-optical patterns for the deep Gulf basin as well as seasonal variation of upper ocean heat energy exchange. Subsequent sections then examine the total spatiotemporal bio-thermal variability within these data. Specifically, an empirical model is developed that describes bio-optical properties as a function of thermal properties. Where the model fails is just as informative as where it succeeds, particularly in terms of identifying episodes of potential shelf water export and river plume influence. Hence the analysis begins with an examination of the seasonal (or background) bio-thermal patterns of the deep Gulf, and then builds upon this foundation in order to isolate and identify other modes of bio-thermal variability.

3. Methods

3.1. SeaWiFS Data

[8] Local area coverage resolution SeaWiFS data for the Gulf of Mexico region (80°W–98°W; 18.8°N–31°N) were collected, processed, and archived at the Naval Research Laboratory (NRL), Stennis Space Center using a SeaSpace Terrascan satellite receiving system and NRL's Automated Processing System [*Martinolich*, 2005], which provided over 60 products derived from ocean color data. However, this analysis was largely confined to the products of the Quasi-Analytic Algorithm (QAA) [*Lee et al.*, 2002], which first decomposes remotely sensed spectral reflectance into total absorption coefficients and total backscattering coefficients over SeaWiFS visible bands (412, 443, 490, 510, 555, and 670 nm; $\Delta\lambda$ = 20 nm). A second suite of empirically based and analytic algorithms then decomposes the total absorption into an estimated absorption by living phytoplankton and absorption by colored detrital matter (CDM). CDM absorption is defined as the sum of colored dissolved organic matter (CDOM) absorption and colored particulate detritus absorption. A list of acronyms is given in Table 1.

[9] In addition, the maximum band ratio algorithm, OC4v4 [*O'Reilly et al.*, 2000], was also used to recover an estimate of surface chlorophyll-*a* concentration (mg m^{-3}), referred to herein as Csat to emphasize that it is the satellite-estimate of surface pigment. An estimate of the blue-light euphotic depth was calculated as 4.6/Kd490, where Kd490 is the satellite estimate of the surface diffuse attenuation of light within the 490 nanometer SeaWiFS band [*Mueller*, 2000]. The satellite algorithms used in this study have been tested elsewhere [*Lee et al.*, 2002; *IOCCG*, 2006; *Bailey and Werdell*, 2006]. Additional information on ocean color algorithm validation, including comparisons against in situ Gulf of Mexico data, is presented in Appendix A.

[10] Three years of these level 3 product files (2002–2004) derived from SeaWiFS local area coverage resolution (~1.1 km) data were sampled to conform to a regular latitude, longitude interval grid of 1/32 degree resolution. Within each 1/32 degree grid, data were rejected if flagged as questionable during processing but not masked from the level 3 product. A postprocessing procedure was developed to remove irregularities in the ocean color data that often appear near the edges of clouds [*Mueller*, 1988; *Yeh et al.*, 1997; *Uz and Yoder*, 2004]. The details are described in Appendix B.

3.2. Modular Ocean Data Assimilation System

[11] The details of the development and implementation of MODAS may be found in *Fox et al.* [2002a]. Briefly, MODAS uses a global grid (1/8°) subsurface climatology of temperature derived from the U.S. Navy's Master Ocean Observation Database (MOODS). MODAS then assimilates remotely sensed SST and sea surface height (SSH) data that have been optimally interpolated [*Bretherton et al.*, 1976] onto a two-dimensional grid. Departure from the subsurface MOODS long-term climatology (all historical observations through 1998 [*Fox et al.*, 2002b]) is then calculated based on regression coefficients that derive subsurface temperature from SSH and SST. The result is a synthetic three-dimensional temperature field.

[12] MODAS was run each day for the upper 300-m of the Gulf of Mexico from January 1, 2002 through December 31, 2004. Both the MODAS temperature profile retrievals and the SeaWiFS data were restricted to the Gulf basin deeper than 300-m (Figure 1), which was determined from the Digital Bathymetry Data Base 2-min resolution (DBDB2) global topography data set. The synthetic temperature profiles were analyzed for three additional variables, which were calculated from each individual MODAS temperature profile before the basin-wide means were computed. First, an index of stratification (STR-30; $\Delta T/\Delta z$) was established by calculating a temperature difference between the surface

Table 1. Acronym List

	Definition
%CDM	Satellite-estimated percent nonwater absorption due to CDM at 443 nm
ACDM	Absorption coefficient for Colored Detrital Matter
APH	Absorption coefficient for Phytoplankton
CDM	Colored Detrital Matter: the sum of colored particulate and colored dissolved nonliving organic matter. The particulate/dissolved distinction is operationally defined as materials that are retained or pass through a 0.2 μm filter.
CDOM	Colored Dissolved Organic Matter
Csat	Satellite estimate of surface chlorophyll-a concentration
CZCS	Coastal Zone Color Scanner
ILD	Isothermal Layer Depth
MLE	Maximum Likelihood Estimator
MODAS	Modular Ocean Data Assimilation System
MP	Mixing Period, as defined in the text
NASA	National Aeronautics and Space Administration
NCEP	National Center for Environmental Prediction
NEGOM	Northeastern Gulf of Mexico Chemical Oceanography and Hydrography Study
NOAA	National Oceanic and Atmospheric Administration
NOMAD	NASA bio-Optical Marine Algorithm Dataset
NRL	Naval Research Laboratory
OC4v4	Ocean Color Algorithm 4 Version 4, for Csat determination
QAA	Quasi-Analytic Algorithm
SeaBASS	SeaWiFS Bio-optical Archive and Storage System
SeaWiFS	Sea-viewing Wide Fields-of-view Sensor
SSH	Sea Surface Height
SST	Sea Surface Temperature
STR-30	Stratification through 30-m, as estimated by MODAS
TE150	MODAS-estimated thermal energy of the upper 150-m
TSP	Thermally Stratified Period, as defined in the text
Z22	MODAS-estimated depth of the 22°C isotherm

and 30-m depth. Second, the isothermal layer depth (ILD) was established by comparing the MODAS temperature at 10-m depth with the first subsequent descending depth where the absolute temperature difference (from 10-m depth) exceeded 0.8°C [*Kara et al.*, 2000]. The ILD was used as a proxy for the depth of the surface mixed layer, since a density-based surface mixed layer calculation would require use of sparse salinity observations. Third, the temperature through 150-m depth was integrated (°C m) and multiplied by a reference density (1027 kg m^{-3}) and the approximate specific heat of seawater (3995 J Kg^{-1} °C^{-1}) at constant pressure to compute the upper ocean thermal energy per unit area (TE150; J m^{-2}). The resulting values, which ranged from ~1.0–1.7 × 10^{10} Joules per square meter, are expressed here as Mega Joules per square centimeter (1.0 × 10^{10} J m^{-2} = 1 MJ cm^{-2}). In the oceanographic literature, this quantity is sometimes referred to as "heat content" [e.g., *Willis et al.*, 2004], which is a proxy for the heat content per unit mass derived from the second law of thermodynamics [*Gill*, 1982].

3.3. Ancillary Data

[13] The net heat flux estimates presented in section 4.1 were averaged over the Gulf from 2.5° latitude, longitude resolution National Center for Environmental Prediction (NCEP) reanalysis data provided by the National Oceanic and Atmospheric Administration's Climate Diagnostics Center from their Web site at http://www.cdc.noaa.gov/. The net heat flux was calculated as the sum for the four NCEP-estimates of the local heat flux components: latent, sensible, shortwave, and longwave.

[14] Nitrate and temperature data presented in section 4.1 are from the Northeastern Gulf of Mexico Chemical Oceanography and Hydrograph Study (NEGOM) cruise data (1998–2000) provided by Texas A & M University from their Web site at http://seawater.tamu.edu.negom/ [see also *Jochens et al.*, 2002]. Additional in situ measurements of chlorophyll and CDM/phytoplankton absorption coefficients were obtained from the NASA bio-Optical Marine Algorithm Dataset (NOMAD) [*Werdell and Bailey*, 2005]. These data are referenced in section 4.1 to support our satellite-based inferences and also used in Appendix A as part of a satellite algorithm validation exercise.

4. Results

4.1. Seasonal Thermal and Bio-Optical Cycles

[15] The seasonal cycle of the MODAS-estimated upper ocean thermal structure across the Gulf may be characterized by two distinct thermal periods. During summer, a surface warm layer greater than 27°C forms within the upper 30-m of the water column (Figure 2a). The mean isothermal layer depth (ILD) during this period occurs at its annual minimum of ~30-m and very close to the maximum vertical thermal gradient (Figure 2a). This gradient is indicative of the shallow seasonal thermocline that is frequently observed in subtropical ocean basins. The Gulf's seasonal thermocline generally erodes in November as the ILD then deepens to ~80-m depth. The time series encompasses four periods of enhanced vertical mixing wherein the maximum vertical thermal gradient deepens to below the 21°C isotherm depth and is indicative of the top of the permanent thermocline (Figure 2a).

[16] The seasonal change in the relationships between the mean isotherm depths and the mean ILD are ecologically important because temperature may serve as a proxy for nitrate concentrations [*Zentara and Kamykowski*, 1977; *Kamykowski and Zentara*, 2003]. Regression of nitrate
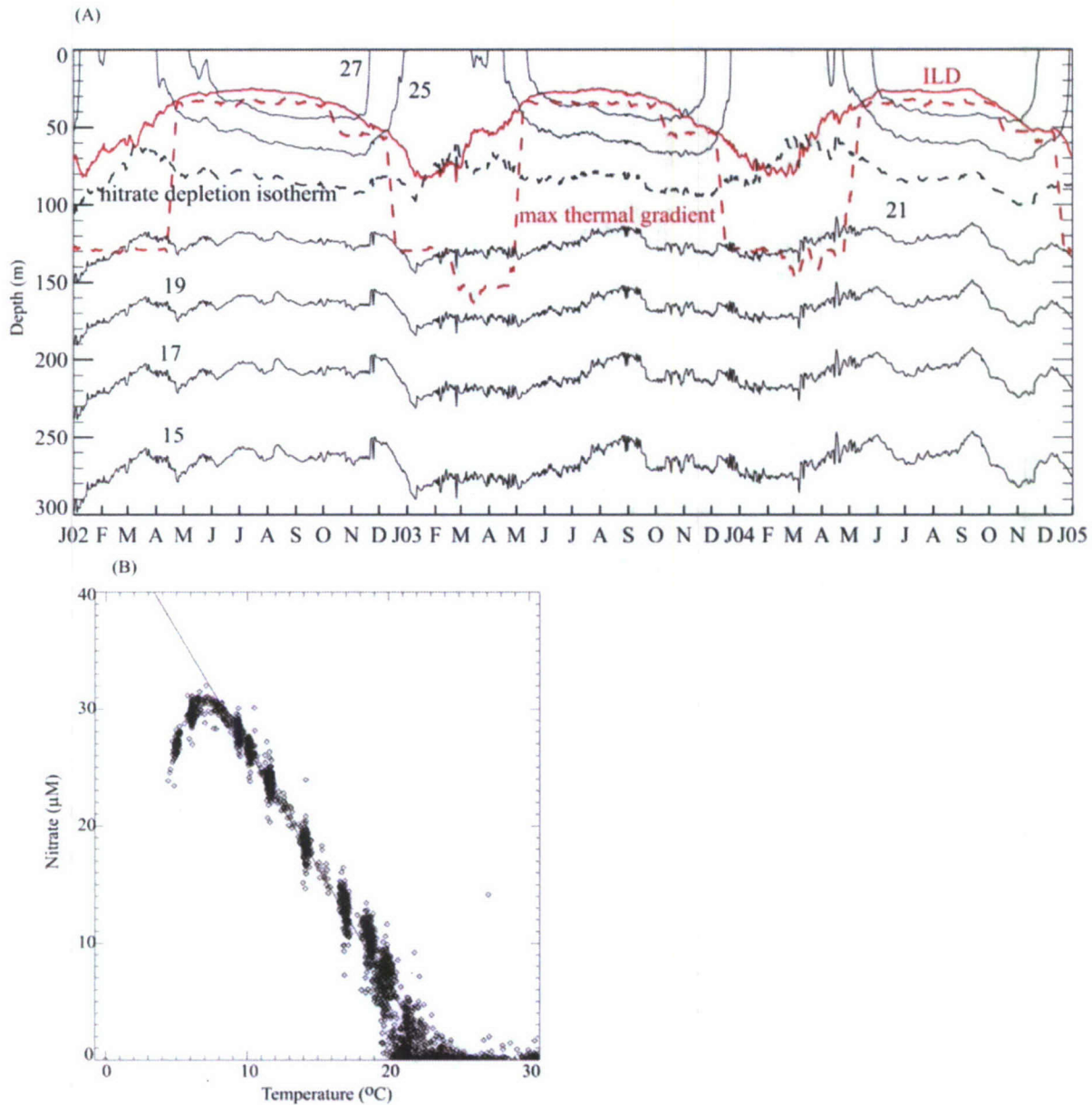
(A)

(B)

Figure 2. (a) The average Gulf-wide daily temperature structure of the upper ocean as estimated by MODAS. The solid red line is the average Gulf-wide isothermal layer depth (ILD). The dashed red line is the depth of the maximum vertical thermal gradient within the upper 300-m calculated from the average vertical temperature profile. The dashed black line is the nitrate depletion isotherm, which was calculated from the data presented in Figure 2b: nitrate versus temperature data from survey cruises in the northeastern Gulf. The linear fit to the nitrate versus temperature data is: nitrate = temp * (−2.023) + 46.9.

versus temperature from discrete depth samples obtained in the northeastern Gulf for stations greater than 300-m depth reveals a linear dependence between nitrate and temperature as well as an estimated nitrate depletion temperature of ~23.2°C (Figure 2b), which is consistent with other observations of temperature and nitrate made elsewhere in the Gulf [*Biggs and Muller-Karger*, 1994; *Zimmerman and Biggs*, 1999; *Biggs and Ressler*, 2001]. It is during the periods of winter mixing that the ILD approaches the nitrate

depletion isotherm, indicative of potential nitrate entrainment into the surface mixed layer. In contrast, the summer ILD and the seasonal thermocline are separated from the nitrate depletion isotherm by a barrier layer some ~40−50 m thick (Figure 2a).

[17] The primary forcing of the seasonal thermal cycle appears to be the reversal of the net ocean-atmosphere heat energy exchange. The 2.5° resolution, daily NCEP net heat flux reanalysis products averaged over the Gulf basin
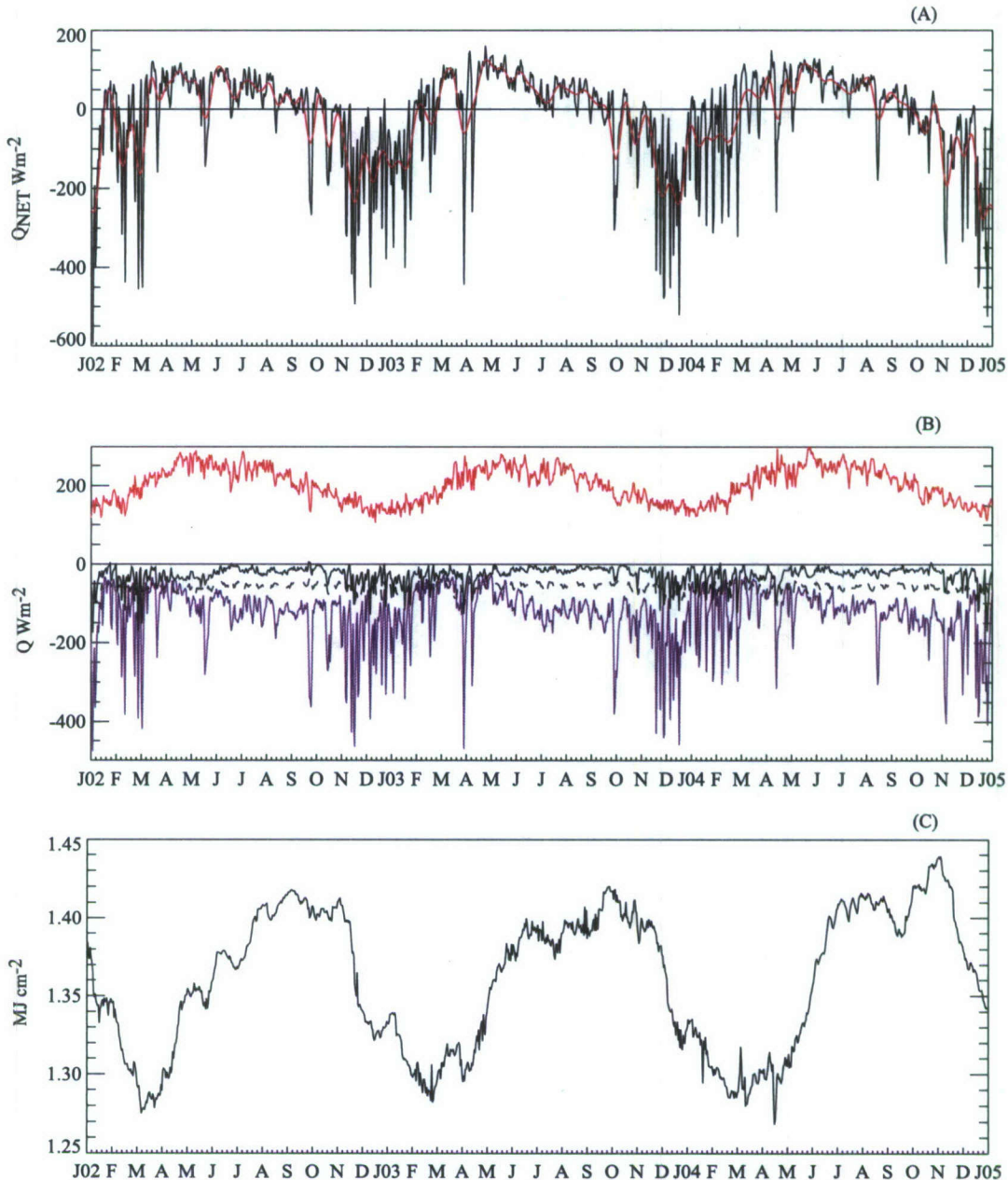
Figure 3. (a) Net heat flux across the air-sea interface (W m^{-2}) for the 3-year time series. Data were averaged from across the Gulf of Mexico using National Center for Environmental Prediction (NCEP) reanalysis data. NCEP reanalysis data were provided by NOAA's Climate Diagnostics Center (http://www.cdc.noaa.gov/). The black line is the daily average and the red line is the low-pass filtered signal. (b) Also shown are the four components of net heat flux given by NCEP averages: net shortwave heat flux (red line), latent heat flux (blue line), longwave heat flux (dashed line), and sensible heat flux (solid black line). (c) The 3-year time series of the daily mean MODAS-generated thermal energy of the upper 150-m (TE150) is also shown.

indicate that the March through September period is one of positive net heat flux (upper ocean heating; Figure 3a). Negative net heat flux (upper ocean cooling) prevails during the remaining months. The NCEP estimate of the four local net heat flux components indicates that it is the vernal increase of shortwave irradiance that raises the net flux above the negative threshold (red line; Figure 3b). Large magnitude ($|\Delta$heat flux$| > 300$ W m^{-2}), high frequency decreases in the latent heat flux then appear to dominate the net heat flux losses during winter (blue line; Figure 3b). Some of these high frequency latent heat flux events may correspond to synoptic-scale increases in surface wind stress associated with the passage of atmospheric frontal systems [*DiMego et al.*, 1976; *Huh et al.*, 1978; *Dagg*, 1988].
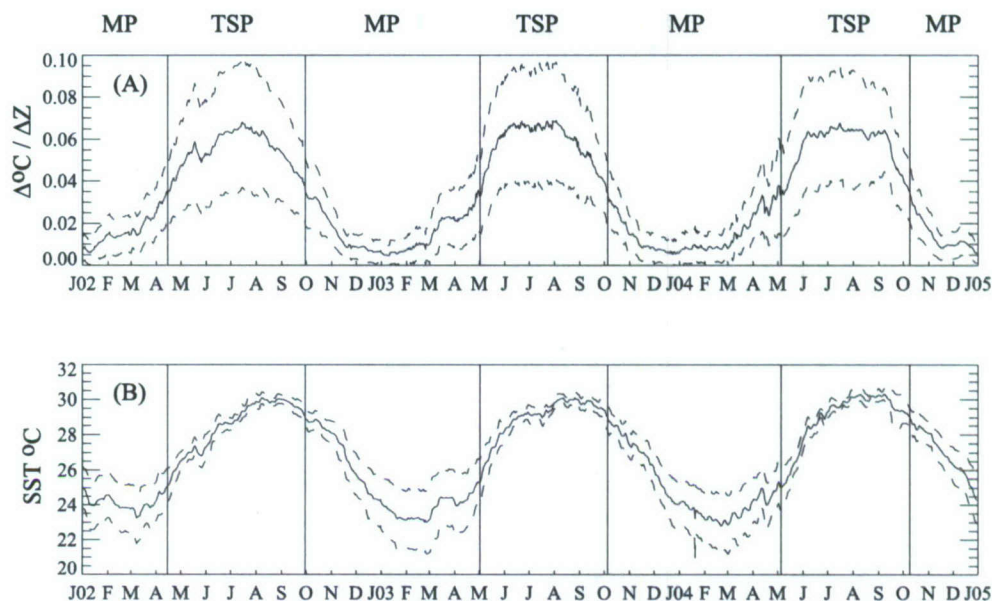
Figure 4. (a) Daily average MODAS-estimated indices of stratification (STR-30: the temperature difference between the surface and 30-m depth); the dashed lines represent the mean ±1 standard deviation. The vertical bars indicate respective periods of mixing (MP) and thermal stratification (TSP), as defined in the text. (b) The mean ±1 standard deviation SST values.

[18] The MODAS-estimated thermal energy of the upper 150-m of the water column (TE150) reflects the combined solar and atmospheric forcing. Minimum mean TE150 values correspond to the transitions from net cooling to net heating, as do the maximum TE150 values correspond to the opposite transitions (Figure 3c). To better delineate the consequences of the divergent temperature and inferred nutrient regimes, the time series was divided into periods based on a thermal criterion of transition above or below 50% of the mean maximum summer stratification value (STR-30). The periods are partitioned by the vertical bars in Figure 4. In this time series, the stratified period (STR-30 > $0.034°C\ m^{-1}$) begins in late April and early May, whereas the mixing period (STR-30 < $0.034°C\ m^{-1}$) begins in late September and early October (Figure 4a) and is matched by a coincident decline in SST's (Figure 4b).

[19] The mean, basin-wide bio-optical signals are likely impacted by the seasonal transitions in thermal structure and ocean-atmosphere heat energy exchange. Summer stratification implies a surface layer (upper 30-m) environment that is both high-light, due to increased shortwave irradiant flux, and low-nutrient due to the large barrier layer between the surface mixed layer and the nitrate depletion isotherm (Figure 2a). Indeed, the stratification period mean Csat values are generally below $0.2\ mg\ m^{-3}$ whereas peaks in mean Csat values range higher than $0.3\ mg\ m^{-3}$ during the mixing period (Figure 5a). These data are also consistent with *Muller-Karger et al.* [1991] mean Gulf Csat fields derived from Coastal Zone Color Scanner (CZCS) data wherein Csat values greater than $0.2\ mg\ m^{-3}$ were observed from December through February, and were generally lower than $0.15\ mg\ m^{-3}$ during other times. Subsequent examinations of CZCS data for the central and western Gulf have revealed the same seasonal cycle [*Biggs and Muller-Karger*, 1994; *Melo González et al.*, 2000].

[20] The ILD during the mixing period did not, however, exceed the mean satellite-estimated blue-light euphotic depth (Figure 5b). This implies that light penetration is sufficiently deep and the depth of the surface mixed layer is sufficiently shallow such that phytoplankton may respond directly to the increased upward nutrient flux brought about by winter mixing and need not endure sub-optimal growth conditions until spring heating increases vertical water column stability. The net result is that the seasonal transition to positive net heat flux during the beginning of the stratification period results in a decrease in surface pigment, as opposed to an increase observed at higher latitudes [*Sverdrup*, 1953; *Sambrotto et al.*, 1986; *Smetacek and Passow*, 1990; *Siegel et al.*, 2002a].

[21] It is thus the annual overturn of the water column across the Gulf that ostensibly stimulates higher phytoplankton biomass, and consequently, higher mean Csat values in an environment where light is not fundamentally limiting to the biota. This is consistent with the proposed mechanism for observed midwinter surface pigment concentration increases in subtropical latitudes described by *Longhurst* [1995] and *Mann and Lazier* [1996]. However, this inferred mechanism may only explain a portion of the seasonal ocean color cycle if one also considers the role of nonliving organic matter. We thus examine the results obtained from the QAA-estimates of phytoplankton and nonliving organic matter absorption to determine what further inferences may be made concerning the Gulf's seasonal bio-thermal cycle.

4.1.1. CDM Absorption

[22] The time series of the Gulf's mean satellite-estimated CDM absorption (at 412 nm) reveals peaks higher than $0.050\ m^{-1}$ during the mixing period, whereas stratification period values are generally less than $0.025\ m^{-1}$ (Figure 6a). The annual doubling of the mean values suggests that
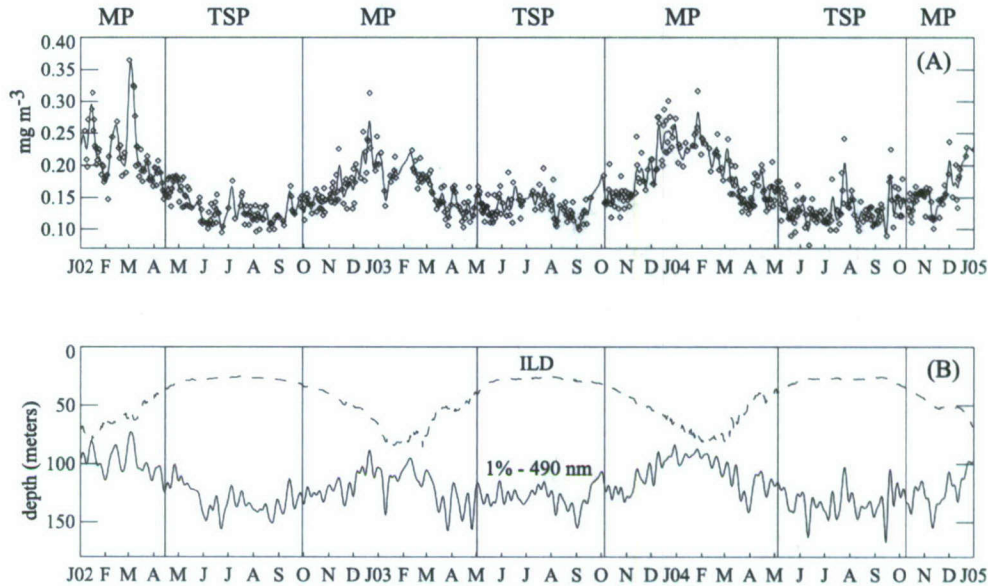
Figure 5. (a) Daily mean SeaWiFS Csat values (OC4v4 algorithm) for the Gulf basin. The solid line corresponds to the linearly interpolated and low-pass filtered signal (Butterworth low-pass filter removed frequencies below 8 days). (b) The daily mean isothermal layer depths estimated by the MODAS fields— dashed line; the solid line is the SeaWiFS-estimated 490 nm euphotic depth calculated from 4.6/(Kd490).

particulate and dissolved forms of nonliving organic matter make significant contributions to seasonal ocean color variability within the Gulf. In order to quantify the relative contribution of CDM versus living phytoplankton to absorption at 443 nm, the percent of nonwater absorption accounted for by CDM (%CDM) was calculated using the expression [cf. *Siegel et al.*, 2005]:

$$\%CDM = \frac{ACDM(\lambda)*100}{ACDM(\lambda) + APH(\lambda)}, \lambda = 443nm \qquad (1)$$

where APH is the QAA-estimated phytoplankton absorption coefficient and ACDM is the QAA-estimated CDM absorption coefficient. The calculated %CDM values ranged between ~45–70% (solid line, Figure 6b). The larger values generally occurred during the mixing period, and the entire data set mean value was 58% (n = 14,958,405).

[23] This value is similar to the one obtained from the Gulf in situ observations (extracted from NOMAD [*Werdell and Bailey*, 2005]) of CDM and phytoplankton absorption:
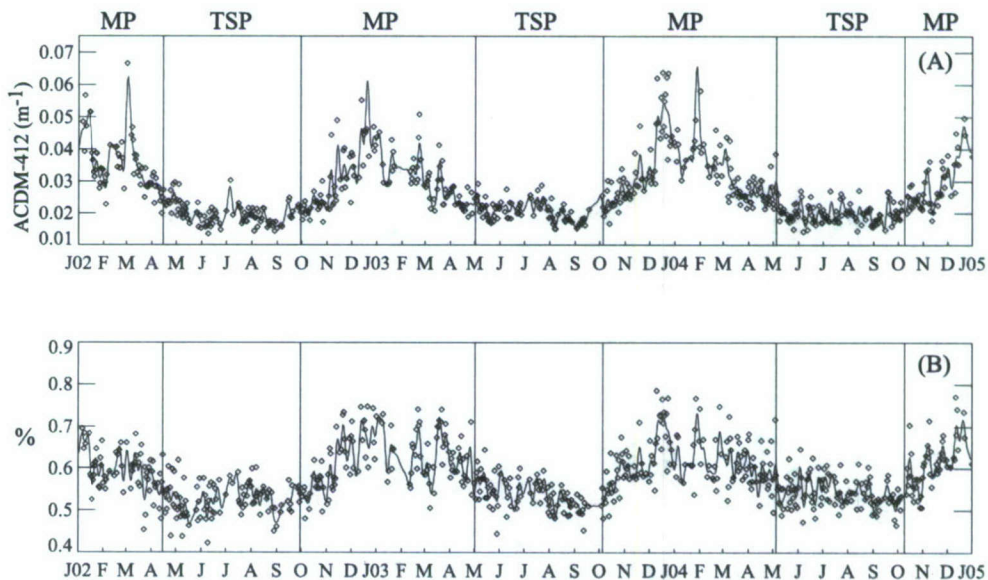

Figure 6. (a) Daily mean SeaWiFS CDM absorption (412 nm) values; the solid line is the low-pass filtered signal. (b) Daily average and low-pass filtered %CDM/100 values.
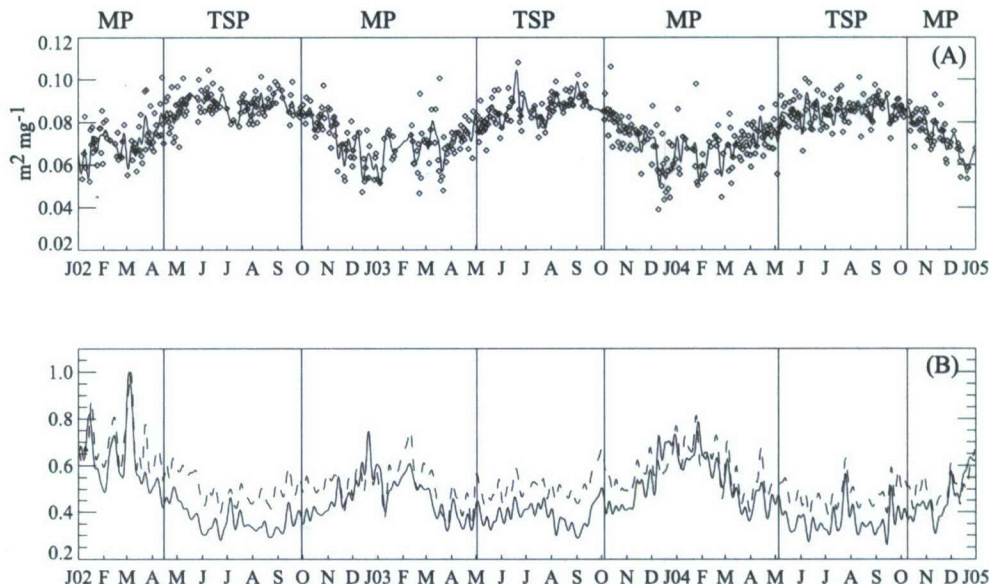
Figure 7. (a) Daily mean SeaWiFS phytoplankton absorption (443 nm) values (QAA) normalized by Csat values (OC4v4 algorithm) for the Gulf basin (satellite a^*). The solid line corresponds to the interpolated and low-pass filtered signal. The mean Csat values were normalized by the maximum value of the time series, and (b) the resulting normalized vector is depicted as the solid line. The dashed line corresponds to the phytoplankton absorption maximum-normalized values.

mean %CDM = 57 (n = 167). To be sure, most of these in situ data were obtained in coastal waters, and some may have been contaminated by estuarine outflows. Nevertheless, if only those samples obtained over water greater than 50-m depth are considered, the majority of blue-light absorption is still due to CDM (mean %CDM = 55, n = 28).

[24] The in situ data and the satellite-based estimates of Gulf %CDM values are also consistent with both observations and satellite estimates made in other ocean basins. For example, *Siegel et al.* [2002b] used a different ocean color algorithm [*Maritorena et al.*, 2002] to estimate a global mean %CDM value of 51.1%. These authors also describe a seasonal %CDM signal in the subtropical Atlantic Ocean ranging from ~45% (summer) to ~70% (winter); a range that is consistent with in situ observations [*Nelson et al.*, 1998]. While this region is not identical to the Gulf, it is nonetheless a subtropical marine environment subject to seasonal cycles of vertical mixing and thermal stratification [*Nelson et al.*, 1998].

4.1.2. Phytoplankton Absorption

[25] A general trend observed in the oceans is that as the surface chlorophyll concentration increases, larger phytoplankton classes become more abundant [*Chisholm*, 1992; *Claustre*, 1994; *Marañón et al.*, 2001; *Li*, 2002]. Based on this general trend, the daily mixing period Csat values exceeding of ~0.25 mg m^{-3} may herald a comparatively larger contribution to total phytoplankton biomass from nano- and microphytoplankton (>2 μm cell diameter), as opposed to the stratification period wherein picophytoplankton (0.2–2 μm) may be more abundant. Seasonal species succession characterized by changes the size structure of the surface phytoplankton community may potentially be diagnosed by examining the relationship between satellite-estimates of phytoplankton absorption and chloro-

phyll concentration [*Sathyendranath et al.*, 2004; *Devred et al.*, 2006]. Absorption efficiency per unit pigment, a^* (m^2 mg^{-1}), tends to decrease in larger phytoplankton cells due to self-shading, i.e., the package effect [*Morel and Bricaud*, 1981; *Kirk*, 1994]. Variability in surface a^* measurements has been shown to be largely a direct consequence of changes in phytoplankton size [*Bricaud et al.*, 2004], although variation of intracellular pigment quantities and the spectral absorption efficiencies of accessory pigments may also play a role [*Bricaud et al.*, 1995; *Cleveland*, 1995].

[26] Hence the surface Gulf waters during the stratification period, a high-light, low-nutrient environment, would likely be populated by smaller phytoplankton with relatively higher apparent absorption efficiencies. The time-series of QAA phytoplankton absorption (443 nm) normalized by Csat (satellite a^*) is consistent with this expectation (Figure 7a). The mean satellite a^* values were nearly 40% higher during the stratification periods. The amplitude of the respective phytoplankton absorption and Csat seasonal signals further emphasizes the potential change in absorption efficiency. During the stratification period, the mean Csat signal was ~40% of the maximum values observed during the mixing period (Figure 7b). In contrast, the phytoplankton absorption values were ~50–60% of their respective mixing period maxima.

[27] The gradations in the relationship between phytoplankton absorption and Csat across the entire region may be better demonstrated with a probability density plot of co-occurrence (Figure 8). Here we examine the possibility of phytoplankton community shifts between the thermal periods by contrasting the observed density distributions in these data with the phytoplankton absorption vs. chloro-
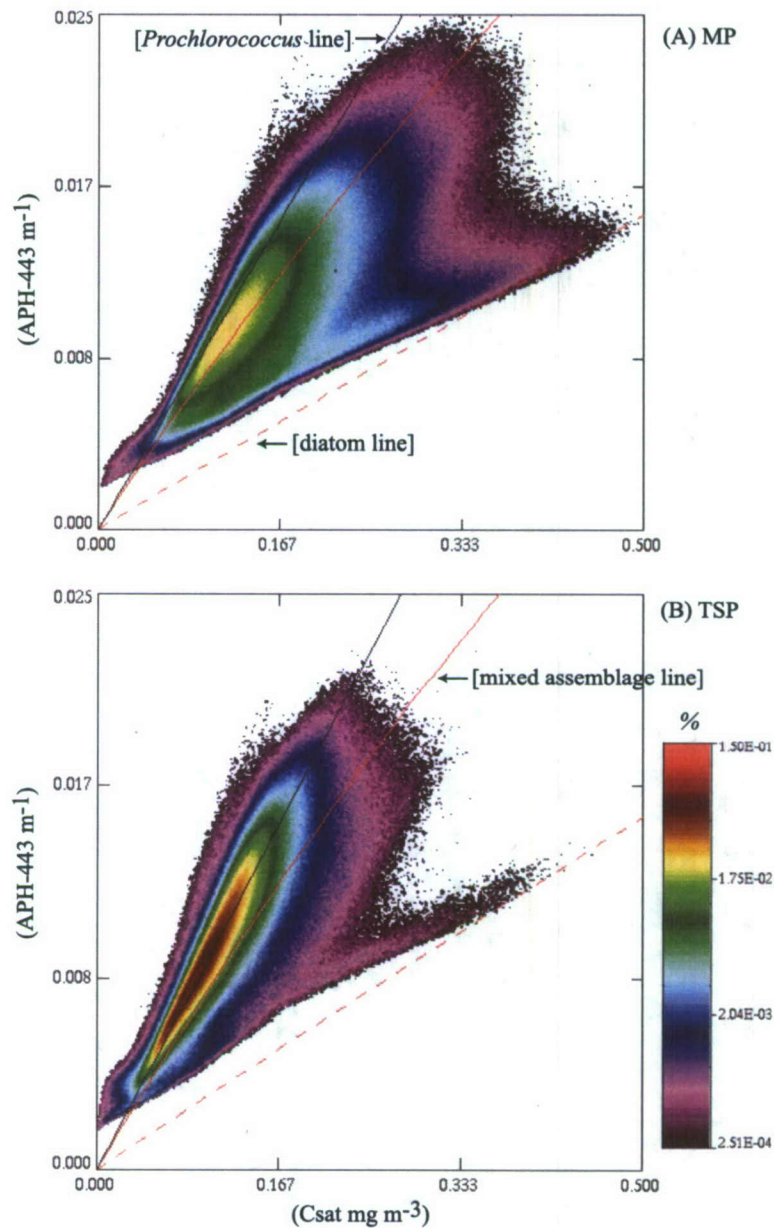
Figure 8. Probability density plots for the co-occurrence of satellite-estimated chlorophyll-*a* concentration and phytoplankton absorption from Gulf of Mexico SeaWiFS data (2002–2004). The "diatom" and "mixed assemblage" lines are constructed for the phytoplankton absorption versus chlorophyll relationships given by *Sathyendranath et al.* [2004]. The *Prochlorococcus* line is a constant $a*$ of 0.09 m^2 mg^{-1}. The values are shown for (a) the mixing periods and (b) the stratification periods. The probability density plots are constructed by dividing the range of values for two variables into 300–400 increments and binning the co-occurrence of the retrieved variable pair into a two-dimensional array. The results of this procedure are then displayed as a percentage: the number of data pairs within each bin divided by the total number of data pairs retrieved. The higher the resolution of the increments, the lower the resulting percentages will be. Probability density plots of co-occurrence are an efficient way to visualize the relationship between two variables retrieved from a very large data set (n > ~10^5).

phyll relationships given by *Sathyendranath et al.* [2004] for a diatom bloom:

$$APH(443nm) = 0.0747\{1 - \exp(-0.27(Csat))\} + Csat(0.0118)$$

(2)

and a mixed assemblage phytoplankton community:

$$APH(443nm) = 0.0281\{1 - \exp(-1.8(Csat))\} + Csat(0.0310)$$

(3)

The mixed assemblage designation was defined by these authors for stations in the Northwest Atlantic that did not meet a pigment biomarker-based criterion. Since this does not necessarily imply a reduced size fraction, an additional *Prochlorococcus* line was added for a constant $a*$ value of 0.09 (m^2 mg^{-1}). This value is from $a*$ measurements of laboratory cultures of *Prochlorococcus*, a ubiquitous prokaryote that is particularly abundant in nutrient-depleted surface waters [*Claustre et al.*, 2002].

[28] During the stratified period, the highest densities of data fall above the mixed assemblage line and coalesce around the *Prochlorococcus* line (Figure 8b). In contrast, the highest data densities during the mixing period fall nearer the mixed assemblage line, with a generally more diffuse distribution (Figure 8a). A greater abundance of larger phytoplankton, inclusive of diatom species, during the mixing period would be consistent with the general observation that larger phytoplankton size classes are more abundant during periods of enhanced vertical mixing [*Harris*, 1986; *Estrada et al.*, 1988; *Valiela*, 1995; *Rodriguez et al.*, 2001]. It is likely that the contours in Figure 8 largely do not meet the diatom line given by *Sathyendranath et al.* [2004] because their data are from diatom blooms wherein the surface chlorophyll concentration ranged from one to two orders of magnitude larger than values typical of the Gulf. Note, however, that the highest Csat values within the data distribution begin to merge with the diatom line (Figures 8a and 8b).

[29] While field studies generally support the inferred link between $a*$ variability and surface phytoplankton community composition [*Bricaud et al.*, 1995, 2004; *Millán-Núñez et al.*, 2004; *Sathyendranath et al.*, 2004], the satellite-based inferences are still subject to uncertainties that arise from the accuracy of the product algorithms applied. The OC4v4 chlorophyll algorithm is an empirical relationship based upon reflectance ratios that, to some degree, are inclusive of changes in surface optical properties such as total absorption, to which phytoplankton absorption is a contributor. This has the potential to introduce some error into the inchoate satellite-based estimate of surface $a*$ variability presented here. Nevertheless, if indeed $a*$ values decline during the mixing period then the Csat values may slightly underestimate the surface chlorophyll field, i.e., there is more chlorophyll for a given quantity of absorption. Since the apparent $a*$ value is the ratio of phytoplankton absorption to chlorophyll-a concentration, a larger chlorophyll value would, in fact, lower the satellite apparent $a*$ value, thus exacerbating the seasonal trend identified here.

[30] On a global scale, dominance of the picophytoplankton is associated with the warm surface waters of the tropical and subtropical oceans [*Agawin et al.*, 2000], where $a*$ values tend to be higher than in other marine environments [*Bricaud et al.*, 2004]. In order to examine the potential relationship between the satellite $a*$ and the thermal fields within these regional data, the probability of co-occurrence data arrays were recast in terms of their thermal properties, i.e., for each corresponding Csat and phytoplankton absorption data pair, the mean SST was calculated.

[31] The result of this procedure revealed that the gradations in apparent absorption efficiency for a given Csat value correspond to gradients in SST (Figures 9a and 9b). During both periods, the warmest average SST's generally correspond to the highest apparent absorption efficiencies. The mean of the corresponding SST values during the mixing period was 24.2°C, whereas the mixing period data corresponding to satellite $a*$ values exceeding 0.09 m^2 mg^{-1} had a mean SST of 25.8°C. Similarly, stratification period satellite $a*$ values exceeding 0.09 m^2 mg^{-1} were, on average, ~0.5 degrees warmer than the Gulf average SST during that interval. These data support the previously established notion that variations in SST are consistent with trends in apparent pigment packaging [*Carder et al.*, 1999].

4.2. Correlation Analysis

[32] The general correspondence between the gradations in satellite $a*$ and SST prompted a more thorough correlation analysis between bio-optical fields and thermal variables. The log-transform of Csat, CDM absorption (412 nm), and satellite $a*$ were compared to five MODAS variables: SST, TE150, ILD, STR-30, and the depth of the 22°C isotherm, Z22. The linear correlation coefficient, r, between the bio-optical and thermal variables was calculated for all matching data pairs within the entire data set as well as during the mixing and stratification periods (Table 2a). The internal correlations between bio-optical or thermal variables were also calculated (Table 2b). In much of the previous section, the average fields were examined in order to focus upon the seasonal variability, thus any information about other modes of variability was lost. Here, however, the correlations are performed on all of the data, and so higher spatiotemporal modes of variability may enter the analysis.

[33] Overall, the data revealed a consistently negative correlation between upper ocean thermal energy (TE150) and Csat, CDM absorption (Table 2a). This comparatively strong correlation ($|r| > 0.4$) persisted during the stratification period when the Csat and CDM absorption to SST correlation coefficients were only ~50% of their respective mixing period values. The difference in the SST correlations between the two thermal periods is a result of the fairly uniform SST's across the Gulf basin during summer months (Figure 4b) that no longer correspond as well to the surface bio-optical variability. As expected, the sign of the satellite $a*$ correlations to TE150 and SST were opposite those of Csat and CDM absorption, implying that pigment packaging, and potentially phytoplankton cell size, is generally reduced in warmer surface waters. The Z22 variable was strongly correlated with TE150, and so its correlation to the bio-optical variables was comparable.

[34] The ILD, however, was weakly correlated to the bio-optical variables ($|r| < 0.4$). Moreover, the sign of the
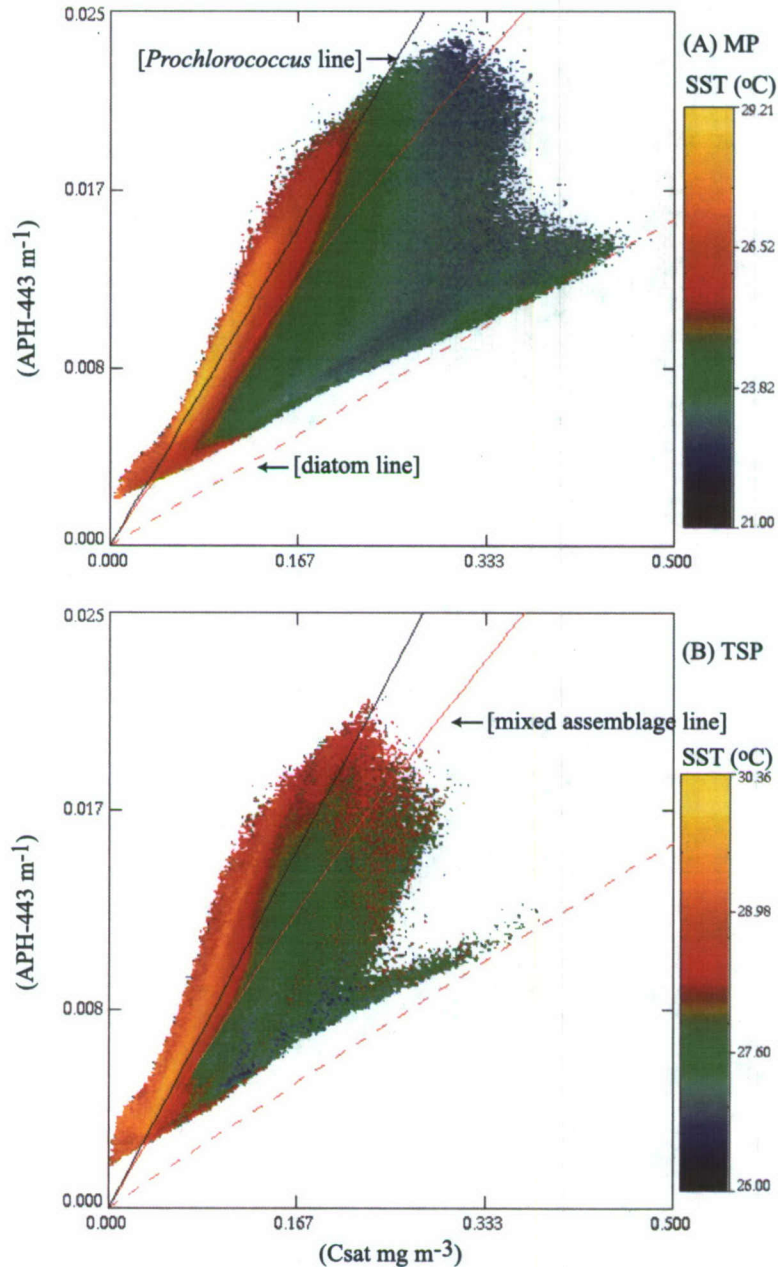
Figure 9. Probability density plots for the co-occurrence of satellite-estimated chlorophyll-*a* concentration and phytoplankton absorption from Gulf of Mexico SeaWiFS data (2002–2004). The mean SST was calculated for each corresponding phytoplankton absorption and Csat data pair for (a) the mixing periods and (b) the stratification periods.

correlation switched between the two thermal periods (Table 2a). The ILD and bio-optical variables are indeed correlated on a seasonal basis; yet, the presence of the Loop Current and other anticyclonic circulation features introduce trends opposite to the seasonal patterns and thereby weaken the correlation strength. This concept may be further demonstrated by contrasting thermal/bio-optical properties along a zonal transect through the Loop Current in the eastern Gulf (Figures 10a and 10b). During January and

September, bio-optical variables along the transect are lower within the Loop Current (as they generally are within other anticyclonic circulation features); the January bio-optical values are also generally higher than those of September (Figure 10a–10d). The ILD, however, is a crude variable that cannot distinguish between isothermal layers of cold, nutrient-replete and warm, nutrient-depleted seawater. Thus the ILD is indeed deeper in January (as bio-optical values are higher), but it is also deeper within the Loop Current (where

Table 2a. Linear Correlation Coefficients Between Log-Transformed Bio-Optical Variables and MODAS Thermal Variables[a]

	TE150	SST	ILD	STR-30	Z22
	Total Correlation Thermally Stratified Period (Mixing Period) n = 14,958,405 n = 5,900,535 (n = 9,057,870)				
Csat	−0.48	−0.49	0.11	−0.13	−0.42
	−0.49 (−0.42)	−0.22 (−0.48)	−0.26 (0.05)	0.35 (−0.14)	−0.45 (−0.39)
CDM-abs.	−0.51	−0.60	0.18	−0.25	−0.43
	−0.48 (−0.46)	−0.24 (−0.55)	−0.24 (0.07)	0.34 (−0.22)	−0.44 (−0.43)
satellite *a**	0.36	0.50	−0.17	0.25	0.31
	0.24 (0.35)	0.18 (0.44)	0.08 (−0.04)	−0.17 (0.19)	0.20 (0.34)

[a]The bio-optical fields are log-transformed because the linear correlation coefficient computation assumes that the underlying probability density functions are normal, and the bio-optical variables tend to be log-normally distributed. Owing to the very large sampling sizes, standard significance testing is superfluous: all of the correlation statistics are significant. The results in the text are discussed instead in terms of "strength" of correlation; the |r| threshold > 0.4 was chosen to describe a strong correlation (bold numbers) because the highest ~40% of the bio-optical to thermal variable correlations exceed this value.

bio-optical values trend lower). Here a comparatively thick layer of warm water accumulates within the convergent center of anticyclonic circulation and isotherms are consequently depressed (Figures 10e and 10f). The SST's are also shown (Figure 10g) to demonstrate how during the stratification periods they are fairly uniform throughout the Gulf.

[35] In contrast to these thermal variables, the CDM absorption and Csat correlations to TE150 remain consistent between the two thermal periods in both sign and magnitude (Table 2a). The seasonal and mesoscale relationships remain consistent between these thermal and bio-optical variables: thermal energy is higher within anticyclonic circulation features, and bio-optical values decline seasonally as mean thermal energy values increase (Figures 10c, 10d, and 10h).

4.3. Thermal Hindcasts of Bio-Optical Fields

[36] This persistent correspondence may be further demonstrated by examination of the subtle differences in the relationship between CDM absorption and TE150 for the two thermal periods (Figure 11). The MODAS-estimated thermal energy for the Gulf time series was divided into 350 increments, and for each increment the mean CDM absorption values were calculated during the thermally stratified period (dashed line, Figure 11a) and the mixing period (solid line, Figure 11a). For both periods, mean bio-optical values decline with increasing thermal energy, as expected from the correlation analysis. However, the slope and cold-core intercept of the linear regression equations are higher

during the mixing period (Figure 11a). The histogram of the thermal energy distribution during both periods (Figure 11b) is shown to emphasize the much smaller sampling size at the peripheries of the distribution, particularly the colder end, where the mean CDM absorption values exhibit more variability and larger standard errors.

[37] The monthly mean CDM absorption values plotted against monthly mean TE150 values further demonstrate the cyclical nature of the seasonal correspondence between the two variables (Figure 11c). March through September mean bio-optical values are lower than October through February mean bio-optical values, given the same quantity of upper ocean thermal energy. Accordingly, if the seasonal bio-optical mean corresponds to the mid-point of the lines shown in Figure 10a, then the bio-optical deviation from that point may be predicted as a function of the local change in upper ocean thermal energy.

[38] This hypothesis was tested by constructing a bio-thermal model to describe the variability in CDM absorption. The regressions of the form $Y = AX^{-B}$, where X is TE150 and Y is CDM absorption (red line, Figure 11a), were chosen because they provide a better fit to the data than a linear regression. Assuming that the regression coefficient, A, behaves similarly to the monthly mean bio-optical values, a sinusoidal relationship was chosen to model its daily change:

$$A = 0.016\sin(0.01721t + 1.364) + 0.0485 \qquad (4)$$

Table 2b. Internal Thermal/Optical Correlation Coefficient Matrices

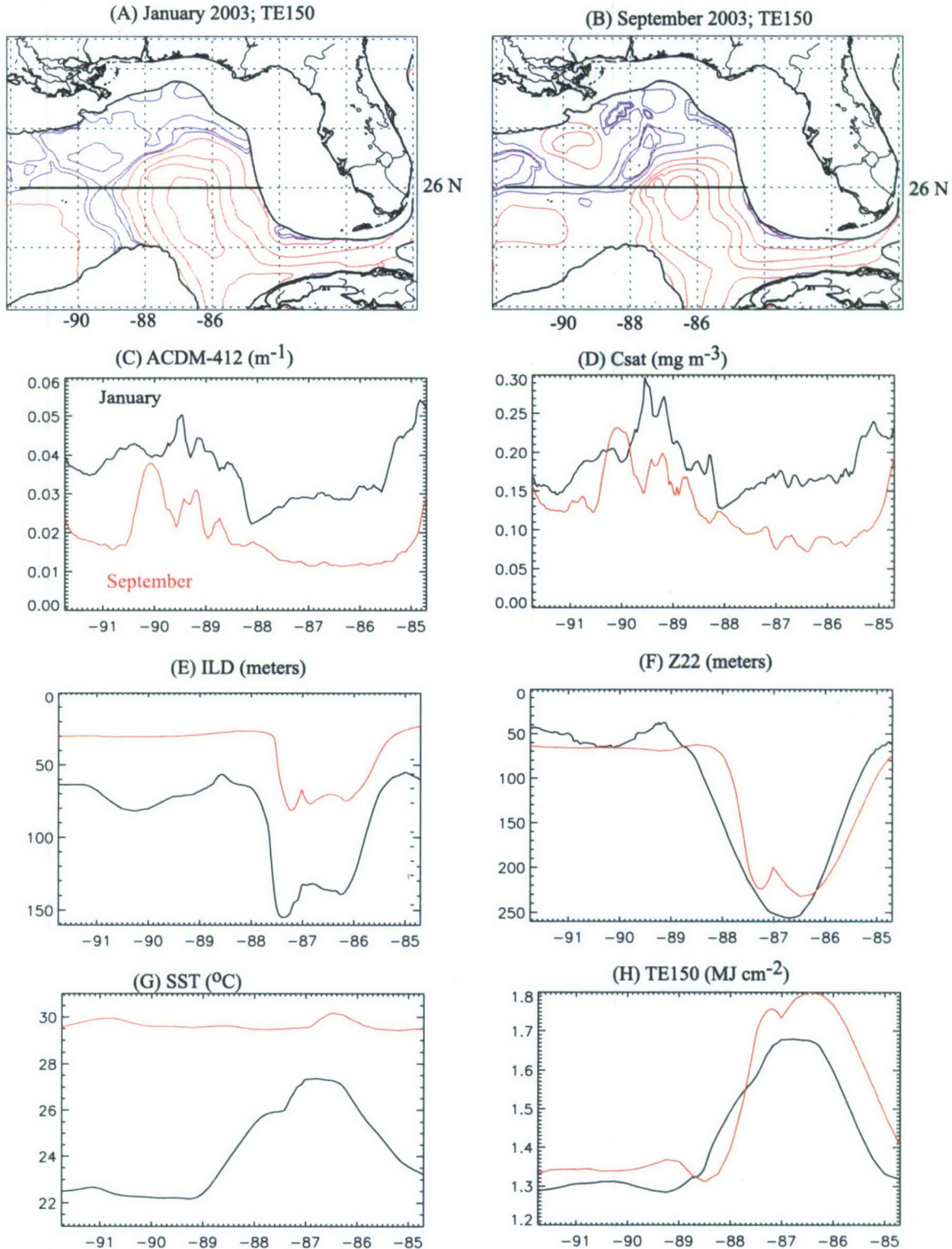|	TE150	SST	ILD	STR-30	Z22
TE150	1	0.59	0.38	−0.21	93
	1	0.38 (0.71)	0.64 (0.49)	−0.67 (−0.33)	0.94 (0.93)
SST		1	−0.33	0.53	0.44
		1	−0.04 (−0.11)	0.24 (0.20)	0.17 (0.62)
ILD			1	−0.68	0.51
			1	−0.65 (−0.73)	0.77 (0.57)
STR-30				1	−0.3
				1	−0.71 (−0.36)
Z22					1
	Csat	ACDM-412	satellite *a**		
Csat	1	0.89	−0.65		
	1	0.90 (0.87)	−0.65 (−0.57)		
CDM-abs.		1	−0.81		
		1	−0.83 (−0.75)		
satellite *a**			1		

Figure 10. Maps of mean TE150 fields for (a) January 2003 and (b) September 2003 are shown with the position of the zonal transect (Figures 10c–10h) extending along 26°N and through the Loop Current. The blue (red) contours correspond to TE150 values below (above) the basin-wide average (1.33 MJ cm^{-2} January and 1.45 MJ cm^{-2} September). The monthly mean values along the transect for (c) CDM absorption, (d) Csat, (e) ILD, (f) Z22, (g) SST, and (h) TE150 are indicated for January (black line) and September (red line) in each panel. The missing values for the bio-optical means were estimated via linear interpolation, and the resulting vector was smoothed using a ~15 km width filter.
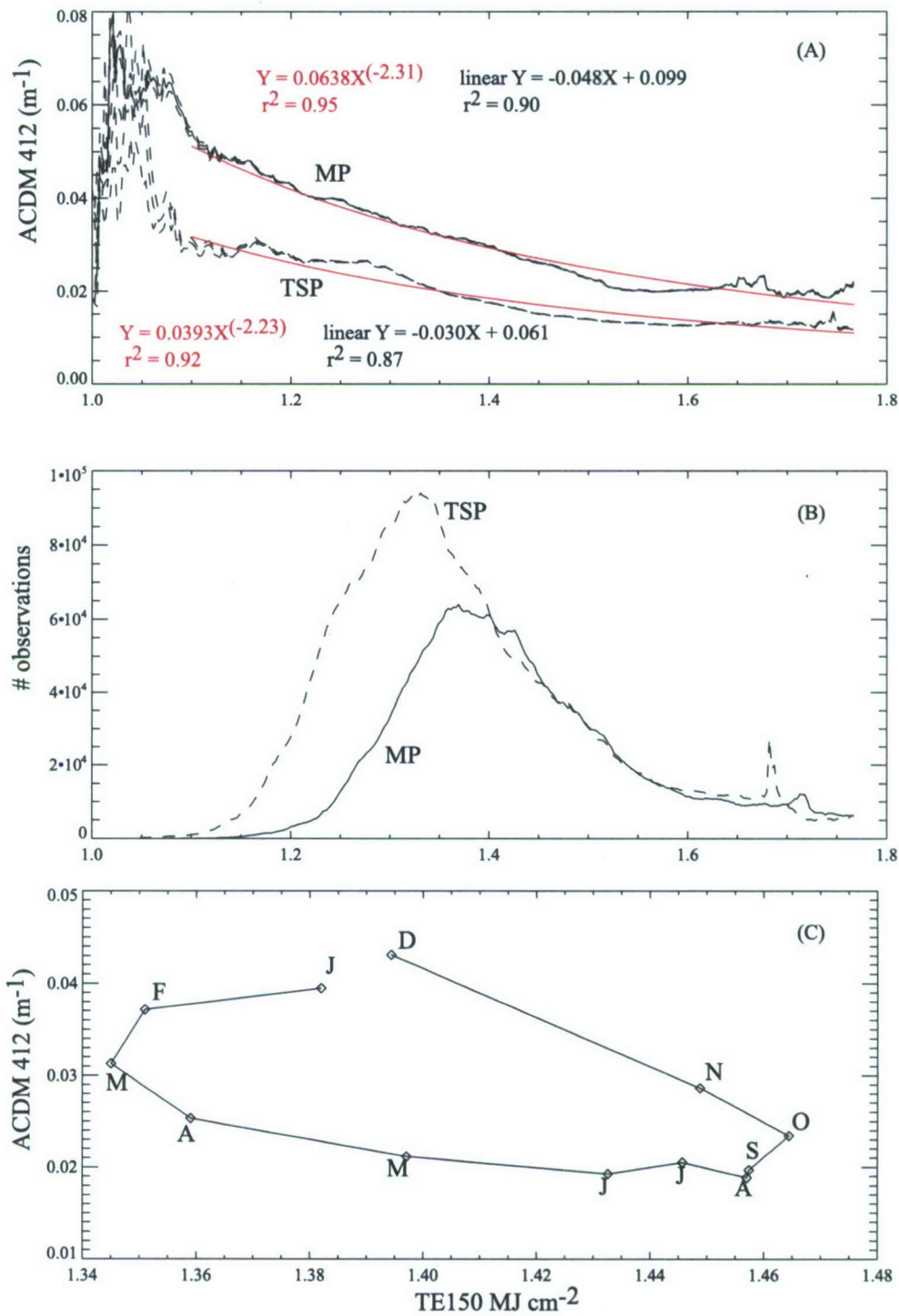
Figure 11. (a) The mean CDM absorption values (ACDM-412) for each thermal energy increment, where $\Delta TE150 = 2.5 \times 10^{-3}$ MJ cm^{-2}, were calculated during the mixing periods (MP) and the thermally stratified periods (TSP). Regressions were performed on mean bio-optical values versus TE150 where TE150 > 1.1 MJ cm^{-2}. The power regressions and resulting r^2 values are indicated in red and the linear regression equations are shown in black. (b) The histogram of TE150 observations during the mixing periods (MP, solid line) and the thermally stratified periods (TSP, dashed line). (c) The monthly mean CDM absorption values versus the monthly mean TE150 values.

Table 3. Thermal Hindcast Error Statistics

	2002–2004 SeaWiFS Data	2005 SeaWiFS Data
	n = 14,958,405	n = 2,955,263
Correlation coefficient	0.67	0.66
Mean percent error	23.82%	23.21%
Mean log-percent error	8.50%	8.40%

where t is the day-of-year. The shift of the sine function was tuned so that the maximum values occurred during the mixing period and the minimum values occurred during the stratification period. The amplitude was empirically adjusted to maximize the resulting correlation between the model and the data. The exponent, B, was held at a constant value (−2.23).

[39] The model results were compared with the original SeaWiFS data set (2002–2004) as well as SeaWiFS data from 2005. In addition to the correlation coefficient, the mean of the percentage error (|model−data|/data) ×100, and the mean of the log-transformed percentage error were calculated. Correlation coefficients between the CDM absorption thermal hindcasts and the SeaWiFS values are high for both the 2002–2004 data set and the 2005 data set (0.66–0.67; Table 3). This is an improvement over the magnitude of the raw correlation between CDM absorption and TE150 (0.51; Table 2a), and is due to the inclusion of the seasonal cycling within the empirical expression. The coefficient of determination between the thermal hindcasts and the satellite data for both time series is ~0.45, suggesting that roughly half of the variance in the CDM absorption fields may be explained by the combined effects of the seasonal cycle and mesoscale thermal variability. Furthermore, the mean percentage errors are less than 25% (Table 3).

[40] The model and satellite CDM absorption histograms reveal how the hindcasts match the lower satellite-estimated CDM absorption values well, but underestimate the higher values (Figure 12a). The map of the largest hindcast underestimates shows that they are clustered in three general areas: the northeast Gulf near the Mississippi River Delta and De Soto Canyon, the northwest Gulf near the Louisiana-Texas Shelf and the northern Mexican Shelf, and the southwestern Gulf in the Bay of Campeche (Figure 12b). The proximity of these areas to the continental shelves suggests that the deviation from the thermal hindcast may be due to the advection of shelf waters into the deep Gulf of Mexico.

[41] Indeed, these same three areas have been previously identified as areas of shelf water export to the deep Gulf [*Muller-Karger et al.*, 1991; *Dowgiallo*, 1994; *Biggs and Muller-Karger*, 1994; *Del Castillo et al.*, 2001; *Morey et al.*, 2003; *Zavala-Hidalgo et al.*, 2003]. Entrainment of low-salinity water associated with Mississippi River discharge into the edges of the Loop Current and associated eddies has been previously inferred from ocean color imagery [*Muller-Karger et al.*, 1991; *Muller-Karger*, 2000; *Del Castillo et al.*, 2001; *Toner et al.*, 2003; *Salisbury et al.*, 2004] and numerical model studies [*Morey et al.*, 2003]. The Bay of Campeche between ~96°W and 93°W was identified by *Zavala-Hidalgo et al.* [2003] as a confluence region where southward along-shelf currents on the Mexican Shelf meet

southwestward currents of the Campeche Bank. Low-salinity discharge from local rivers may be exported off shelf here as well. These authors also identified the southwestern Louisiana-Texas shelf as another confluence region, although other authors have noted potential interactions of anticyclonic-cyclonic eddy pairs with the shelf in this same area [*Biggs and Muller-Karger*, 1994].

[42] Composite SeaWiFS imagery further reveals potential shelf water export events. During the spring of 2003, MODAS thermal fields indicate a cold-core and warm-core eddy pair in the western Gulf adjacent to the southwestern Louisiana-Texas Shelf (Figure 13c). SeaWiFS data indicate an apparent filament of high CDM absorption water was advected off shelf in between these two features (Figure 13a). The thermal hindcast CDM absorption values do not capture this feature, but do otherwise generally mimic the contrast between the anticyclonic circulation features and the remaining Gulf (Figures 13a and 13b). The summer 2004 thermal hindcast further mimics the seasonal decrease in surface CDM absorption values apparent in the SeaWiFS imagery as well as the persistent contrast between warm-core and cold-core circulation centers (Figure 14). Here again, however, large errors occur near the shelves. This is particularly the case in the northeast Gulf between the Loop Current, here extended north of 27° latitude, and the shelf where CDM absorption values exceeding 0.05 m^{-1} appear. Mismatches between the SeaWiFS data and the thermal hindcasts also occur along the Louisiana-Texas Shelf and in the Bay of Campeche (Figures 14a and 14b).

5. Discussion

5.1. Seasonal Bio-Thermal Patterns

[43] Our inference of the Gulf's seasonal bio-thermal cycle from these satellite data is consistent with previous studies of this basin [*Walsh et al.*, 1989; *Muller-Karger et al.*, 1991]. The period of winter mixing and thermal energy loss from the surface ocean to the atmosphere is accompanied by an increase in near-surface chlorophyll concentration. The mechanistic hypothesis is that light penetration is sufficiently deep and mixing depth, although increased, is nonetheless still sufficiently shallow such that light-limitation of the phytoplankton does not generally occur; phytoplankton may immediately assimilate nutrients entrained into the surface mixed layer. Thermal stratification then occurs during the spring transition to net upper ocean heating, and this process restricts the surface mixed layer from deep-ocean nutrients. The resulting high-light, low-nutrient surface environment is then characterized by a decline in surface chlorophyll concentration.

[44] The comparison of seasonal chlorophyll concentration trends for the deep Gulf with the QAA-estimated phytoplankton absorption coefficients further suggests an additional change in the phytoplankton absorption efficiency (a^*) that may result from a shift in the surface phytoplankton community composition. This satellite-based inference is consistent with in situ observations. *Qian et al.* [2003] examined phytoplankton pigment distributions between the Mississippi River and Tampa Bay. While their study was largely confined to the continental shelf, these authors report that the proportional prokaryote abundance on the outer shelf and slope stations declined during the winter cruises. Fur-
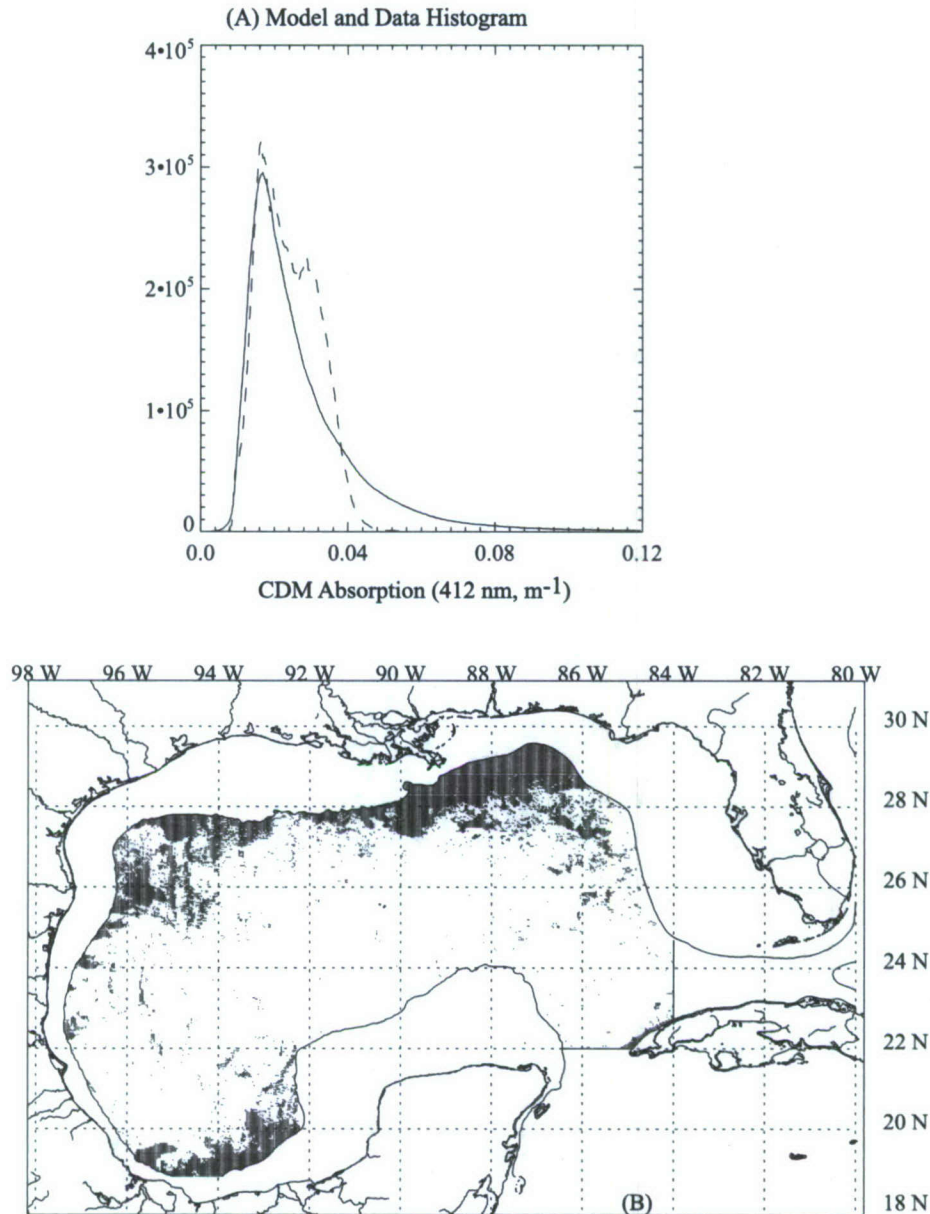
Figure 12. (a) Comparison of histograms of satellite CDM absorption (ACDM-412) distribution (solid line) and modeled ACDM-412 distribution (dashed line). (b) The map of where the log-transformed percent error between model and data [(data − model)/data * 100.0] exceeded 100%.

thermore, analysis of chlorophyll fractionation, phytoplankton species counts, and pigment biomarkers made during the 1992–1994 Louisiana-Texas Shelf Circulation and Transport Process Study confirm that pico- and nanophytoplankton (<20 μm cell diameter) comprised the majority of deep water phytoplankton, except during the winter cruise when large diatoms were instead abundant [*Lambert et al.*, 1999; *Biggs and Ressler*, 2001, and references therein].

[45] In addition to phytoplankton absorption trends, a strong seasonal correspondence was identified between the satellite estimates of %CDM, the CDM absorption coefficient, and surface chlorophyll. This finding is of particular importance because the processes constraining chlorophyll concentration may not be the same as those constraining CDM absorption. In situ data from the Gulf [*Werdell and Bailey*, 2005] and other ocean basins [*Siegel et al.*, 2002b] indicate that the majority of CDM absorption is due to the dissolved rather than the particulate phase. Thus the discussion of CDM absorption variability may be further illuminated by an examination of the potential sources and sinks of colored dissolved organic matter (CDOM) in the surface waters overlying the deep Gulf. For greater clarity, we discuss CDOM first in terms of potential autochthonous sources from within the deep Gulf, and
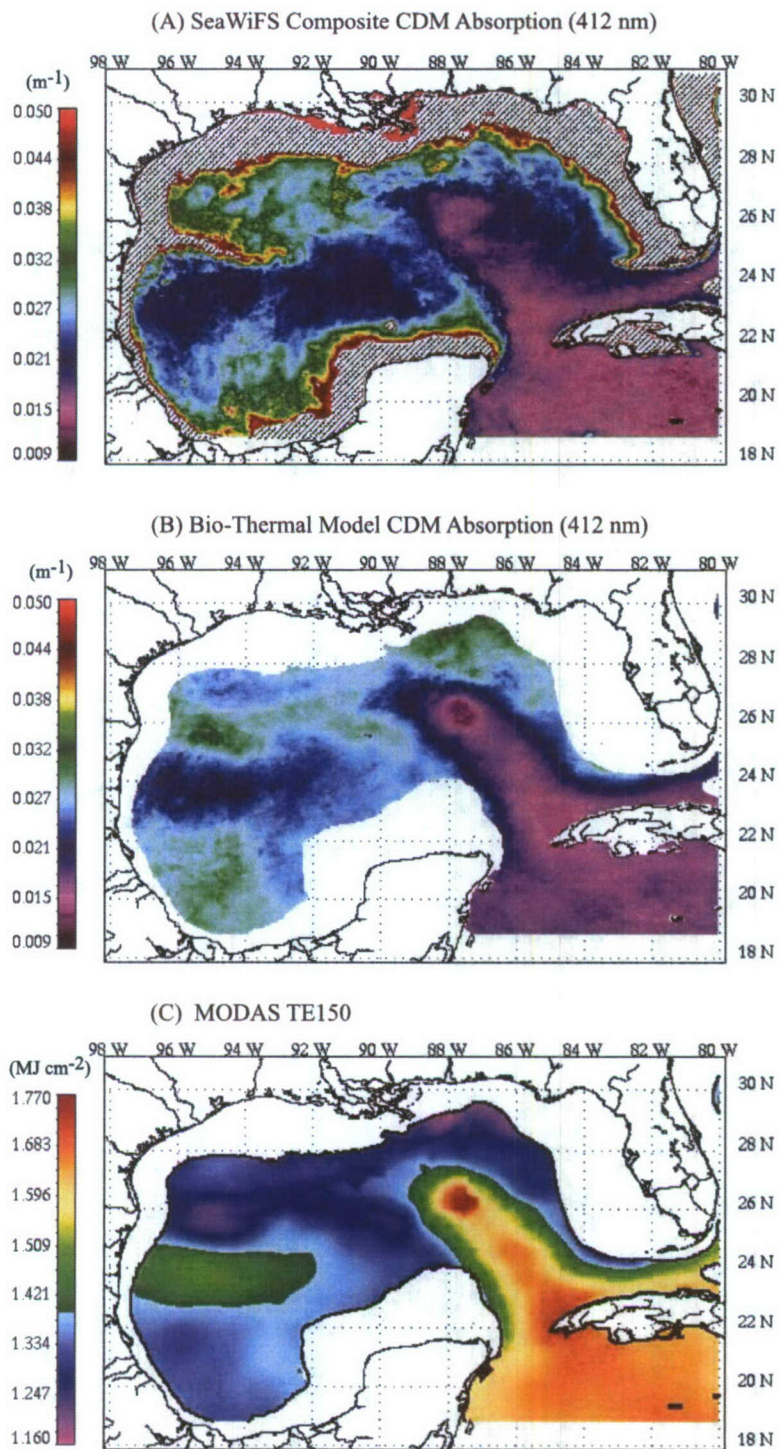
Figure 13. (a) The composite SeaWiFS image for 2003, March–May; (b) thermal hindcast CDM absorption (ACDM-412) values; (c) MODAS upper ocean thermal energy. For Figure 13a all ACDM-412 values exceeding 0.05 m^{-1} are contoured by the horizontally hatched region. SeaWiFS composite images were constructed by calculating the mean (see equation (B1)) for each grid location; clouds or missing data were excluded. The model CDM absorption values were resampled at the same frequency as the SeaWiFS data.

(A) SeaWiFS Composite CDM Absorption (412 nm)

(B) Bio-Thermal Model CDM Absorption (412 nm)

(C) MODAS TE150

Figure 14. (a) The composite SeaWiFS image for 2003, July–September; (b) thermal hindcast CDM absorption (ACDM-412) values; (c) MODAS upper ocean thermal energy. For Figure 14a all ACDM-412 values exceeding $0.05 \ m^{-1}$ are contoured by the horizontally hatched region. SeaWiFS composite images were constructed by calculating the mean (see equation (B1)) for each grid location; clouds or missing data were excluded. The model CDM absorption values were resampled at the same frequency as the SeaWiFS data.
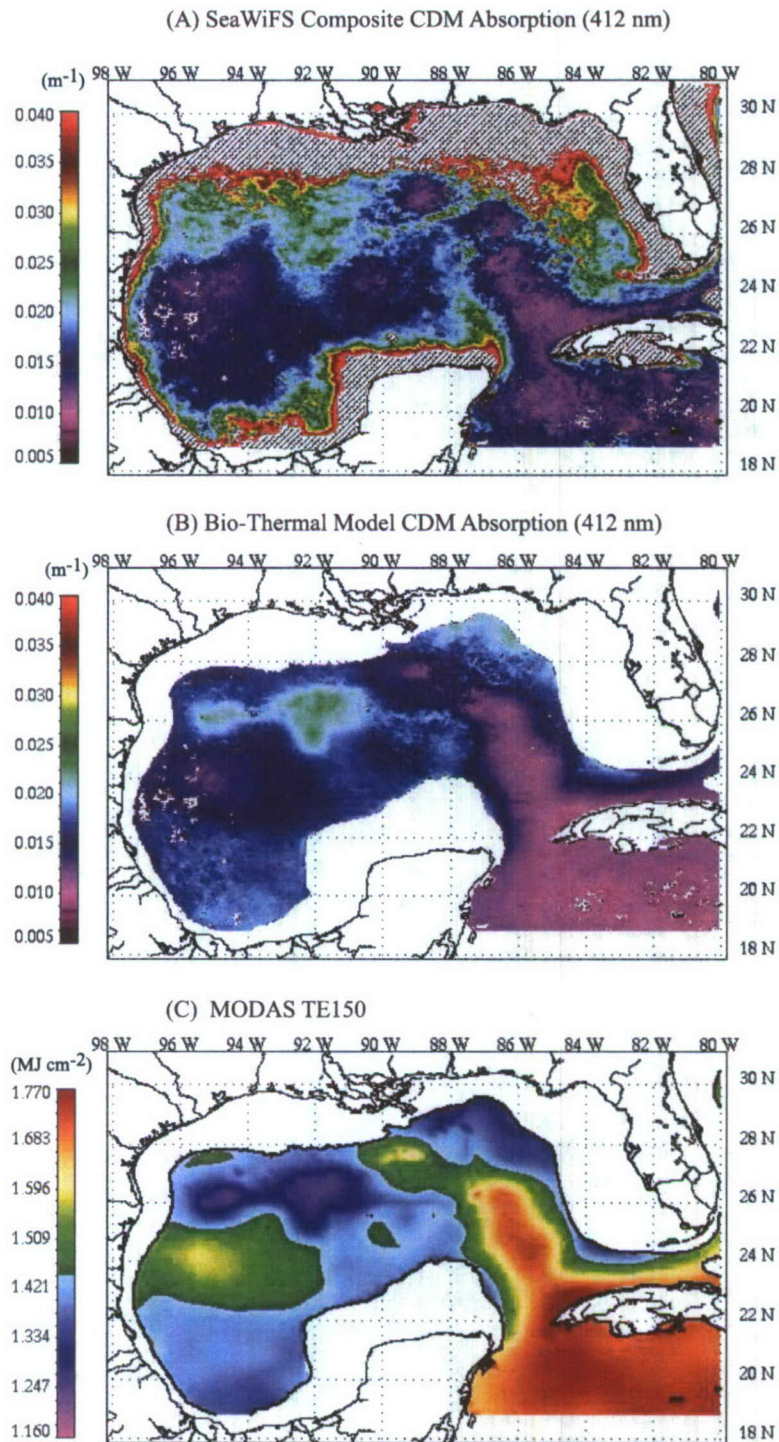
reserve the discussion of allochthonous materials for the section on lateral advection (5.2).

[46] CDOM has been previously described as the "wastewater" left behind from past oceanic processes [*Siegel et al.*, 2002b]. The exact pathways of CDOM production are not clear, although there is evidence that CDOM is produced via bacterial degradation of noncolored organic matter derived from phytoplankton [*Rochelle-Newall and Fisher*, 2002; *Nelson et al.*, 2004]. Regardless of the specific pathways of production, primary productivity presumably leads to an accumulation of wastewater and this implicates two in situ CDOM sources: (1) increased CDOM production in winter as a consequence of elevated levels of primary productivity; and (2) the deep chlorophyll maximum, often observed in subtropical basins below the seasonal thermocline and near the nitrate depletion isotherm, may also be a location of CDOM accumulation during the stratified periods, and these materials are subsequently brought to the surface during the winter overturn. This latter mechanism was proposed to explain the observed seasonal CDOM cycle in the Sargasso Sea near Bermuda [*Michaels and Siegel*, 1996; *Nelson et al.*, 1998], and other tropical/subtropical latitudes [*Chen and Bada*, 1992; *Coble et al.*, 1998; *Siegel et al.*, 2002b; *Simeon et al.*, 2003]. In the Gulf, the large seasonal barrier layer between the stratification period ILD (~30-m) and the nitrate depletion isotherm (~70-m; Figure 2a) may be such a location of CDOM accumulation. Subsurface CDOM maxima coincident with chlorophyll-*a* maxima have indeed been observed in the Gulf [*Chen et al.*, 2004]. To be sure, however, CDOM production in the deep ocean may also arise from the decomposition of nonliving organic matter over much longer timescales than the seasonal cycle emphasized here [*Nelson et al.*, 2007].

[47] Phytoplankton are consumed by herbivores, particulates may sink, yet there must be some additional removal process to account for seasonal CDOM depletion, particularly since CDOM largely consists of humic substances that may be recalcitrant to microbial consumption. The most likely removal process candidate is photochemical degradation [*Mopper et al.*, 1991; *Moran and Zepp*, 1997; *Mopper and Kieber*, 2000; *Del Vecchio and Blough*, 2002]. Photochemical degradation may entail the direct oxidation of CDOM to dissolved inorganic carbon, the formation of other potentially smaller and more labile organic compounds, or the alteration of CDOM optical properties, i.e., photobleaching.

[48] Collectively, these photochemical processes act to reduce apparent CDOM absorption coefficients and may further explain the persistent relationship identified between CDM absorption and upper ocean thermal energy if one considers that the increased vernal shortwave irradiant flux (red line, Figure 3b) may have both photochemical and thermal consequences. The increased irradiant flux results in net upper ocean heating (positive net heat flux; Figure 3a), and the thickness of the surface mixed layer is consequently reduced (Figure 2a). Colored dissolved materials become confined to this restricted surface layer as they are simultaneously exposed to an increasing intensity of ultraviolet (UV) irradiance (280–400 nm), which is the spectral range that largely stimulates photochemical processes [*Kieber*, 2000]. As summer stratified conditions progress, UV-stimulated

CDOM depletion may rapidly outpace CDOM production within the increasingly warm and nutrient-depleted surface waters. Conversely, a winter decline in the total irradiant flux, combined with wind-driven (latent) losses of heat energy, may stimulate convective overturn and turbulent mixing. Primary productivity increases during this period with the potential for a proportional increase in the CDOM production rate relative to that of CDOM depletion.

[49] Despite these potentially divergent constraints for CDM absorption and chlorophyll, the two variables are nonetheless highly correlated (Table 2a). A potential explanation for this tight CDM-chlorophyll coupling is that photoadaptation of surface phytoplankton may decouple some of the apparent variability in chlorophyll from changes in phytoplankton biomass, as has been previously suggested for subtropical ocean basins [*Siegel et al.*, 2005]. Indeed, phytoplankton carbon to chlorophyll ratios, a proximate indicator of the photoadaptive response, may vary by a factor of six or more [*Geider*, 1987; *Sakshaug et al.*, 1989; *MacIntyre et al.*, 2002]. Given that CDM absorption appears to account for the majority of constituent blue-light absorption in the Gulf and in much of the global oceans [*Siegel et al.*, 2002b], we may speculate that increasing intracellular quantities of chlorophyll (as a photoadaptive response to a light field largely attenuated by CDM) may further reduce the phytoplankton absorption efficiency due to the package effect [*Morel and Bricaud*, 1981; *Kirk*, 1994]. Accordingly, there may be a subtle interaction between chlorophyll, phytoplankton absorption efficiency, and CDM absorption that is discernable within satellite data.

5.2. Mesoscale Circulation and Lateral Advection

[50] Our seasonal mechanistic inferences are intentionally described thus far in a one-dimensional (vertical) context. The role of lateral advection becomes clearer as one considers the mesoscale variability. The Loop Current delivers surface waters to the Gulf from the Caribbean Sea that are comparatively lower in chlorophyll concentration [*Muller-Karger et al.*, 1989; *Bidigare et al.*, 1993; *Melo González et al.*, 2000]. This pattern persists into the mesoscale (~months, hundreds of kilometers) because isotherms, and by inference nutrient isopleths, are depressed within the centers of convergent circulation. In contrast, isotherms are uplifted within divergent, cyclonic circulation features, resulting in local "biological oases" [*Biggs and Ressler*, 2001], i.e., local areas of enhanced primary productivity.

[51] Analogously, our satellite estimates of CDM absorption coefficients in the surface waters of the northwestern Caribbean Sea are generally ~25% lower than those estimated for the surface waters overlying the deep Gulf. Given that both the total irradiant flux and UV intensity increase towards the equator [*Whitehead et al.*, 2000], it is not surprising that an initially poleward flowing surface current would deliver comparatively high-thermal energy, low-CDOM waters. Since there is ostensibly no significant CDOM source within convergent circulation features due to depressed nutrient isopleths and, consequently, a depressed rate of primary productivity, this pattern is maintained within the Gulf. Indeed, humic substance concentrations in the Loop Current are much lower than those typically observed elsewhere in the Gulf [*Harvey et al.*, 1983; *Carder et al.*, 1989]. In contrast, the biological

oases provided by cyclonic eddies may also be local areas of CDOM production; although entrainment of deeper high-CDOM waters into the surface mixed layer may also occur. Here again, the tight CDM absorption to chlorophyll coupling may be due, in part, to a photoadaptive response.

[52] Further deviations from these patterns may indicate lateral advection of shelf waters or potential interactions of the deep Gulf with the continental shelf/slope. The Mississippi River plume, the Suwannee River plume, and other rivers and estuaries have a notable impact upon the Gulf's coastal ocean color variability and have been implicated in shelf water export events [*Muller-Karger et al.*, 1991; *Gilbes et al.*, 1996; *Muller-Karger*, 2000; *Del Castillo et al.*, 2001; *Gilbes et al.*, 2002; *Jolliff et al.*, 2003; *Toner et al.*, 2003]. Furthermore, coastal river plumes generally have CDOM absorption values one or more orders of magnitude larger than those observed in the deep Gulf [*Green and Blough*, 1994; *Del Castillo et al.*, 2000; *Hu et al.*, 2003]. Whether these allochthonous colored dissolved materials mix conservatively into the deep Gulf or are instead subjected to rapid photochemical degradation within buoyant surface plumes [*Kieber et al.*, 1990; *Miller and Zepp*, 1995; *Amon and Benner*, 1996; *Hedges et al.*, 1997; *Vodacek et al.*, 1997; *Andrews et al.*, 2000; *Morell and Corredor*, 2001; *Del Vecchio and Blough*, 2002; *Jolliff et al.*, 2003] warrants further study.

[53] Nevertheless, the potential role of freshwater effluent in our basin-wide analysis of the deep Gulf deserves additional clarification. The Mississippi River drains 41% of the conterminous United States (the third largest drainage basin in the world [*Van der Leeden et al.*, 1990]) and is responsible for the majority of the total freshwater discharge into the Gulf basin [*Dunn*, 1996; *Goolsby et al.*, 2001]. Seasonal peaks in Mississippi River discharge rate often occur in spring (March–May [*Walker*, 1994]), and maximum seasonal CDOM absorption values associated with low-salinity plumes around the Mississippi River Delta extend well into the summer (July–August [*Hu et al.*, 2003]). This pattern appears to be out of phase with the seasonal thermal/CDM absorption cycle for the deep Gulf identified here.

[54] Thus export of freshwater effluent to the deep Gulf may be tentatively identified in the satellite record as anomalous deviations from the expected bio-thermal patterns. For example, the daily mean CDM absorption values (as well as the bio-thermal model hindcast values) are extracted for the continental slope (300–2000 m depth) immediately south of the Louisiana and Mississippi coasts (Figures 15a and 15b). Although the potential influence of river plumes during the mixing periods cannot be excluded, the seasonal pattern of elevated CDM absorption values during winter months is consistent with the Gulf-wide bio-thermal variability as well as the local NCEP estimate of latent heat flux, and by inference, vertical mixing (Figures 15b and 15c). In contrast, increasing thermal stratification and shortwave irradiance (Figure 15c) should correspond to lower CDM absorption values, consistent with the photochemical CDOM depletion hypothesis. This is clearly not the case during the summers of 2003 and 2004 when significant deviations from the expected patterns occur (Figure 15b). It is likely that these anomalous CDM

absorption peaks do, in fact, correspond to episodes of low-salinity water (<34 PSU) export to the deep Gulf.

[55] There may also be a more subtle correspondence between these bio-optical anomalies and the thermal fields. Enhanced thermal stratification during summer (Figure 15d) may effectively decouple surface and bottom frictional boundary layers over the shelf—thereby enhancing Ekman drift in the surface layers [*Kudryavstev and Soloviev*, 1989; *Savidge*, 2002] and increasing the cross-shelf extent of water mass exchange [*Lentz*, 2001]. In addition to eddy intrusion over the continental slope, this stratification effect may augment summer time off-shelf river plume dispersal in the northern Gulf [*Walker*, 1996; *Salisbury et al.*, 2004]. Indeed, entrainment of low-salinity waters into deep Gulf mesoscale circulation features appears to be much more frequent during the thermally stratified periods [*Morey et al.*, 2003]. Thus it would appear that if the Mississippi River was the dominant source of colored dissolved materials to the deep Gulf, the seasonal CDM absorption and %CDM cycles should instead peak during the stratified periods. Since this appears not to be the case (Figure 6), the seasonal bio-thermal patterns identified herein likely arise from the cycling of autochthonous materials. Furthermore, fluxes of heat and fluvial freshwater into the deep Gulf may have distinctly opposite bio-optical consequences, and these fluxes may potentially be assessed using satellite-based data sets.

6. Conclusions and Implications

[56] Elevated winter surface chlorophyll concentrations, CDM absorption coefficients, and potentially reduced phytoplankton absorption efficiencies concomitant with upper ocean thermal energy losses and increased depths of mixing, followed by opposite trends during spring and summer, appear to constitute a robust seasonal bio-thermal cycle for the deep (>300-m depth) Gulf of Mexico. Hence the combined thermal and bio-optical data set suggests a sequence of interrelated events that entail changes in the dynamic balance between heat flux terms, the impact of these changes upon the temperature and density structures of the upper ocean, and the effects of these processes upon the cycling of organic matter. Specifically, a vernal increase in shortwave irradiant intensity appears dominate the other heat flux terms and result in a positive net heat flux such that the surface ocean begins to gain heat energy. While both temperature and salinity fields impact density fields, we presume that in the open Gulf net surface heating generally increases vertical density gradients and may, in turn, further result in increasing vertical gradients of organic matter concentration. This latter effect will be particularly acute if the rates of production and consumption of these organic materials are also subject to vertical variations across the thermally imposed density gradients.

[57] Vertical variations in upper ocean rate processes pertinent to the cycling of organic matter are often cast in terms of the respiration and photosynthesis of phytoplankton communities, i.e., the critical depth theory, and this concept is certainly consistent with the data presented here. The penetration of shortwave irradiance into the winter water column is perhaps sufficiently deep to sustain elevated chlorophyll concentrations (and by inference elevated rates of photosyn-
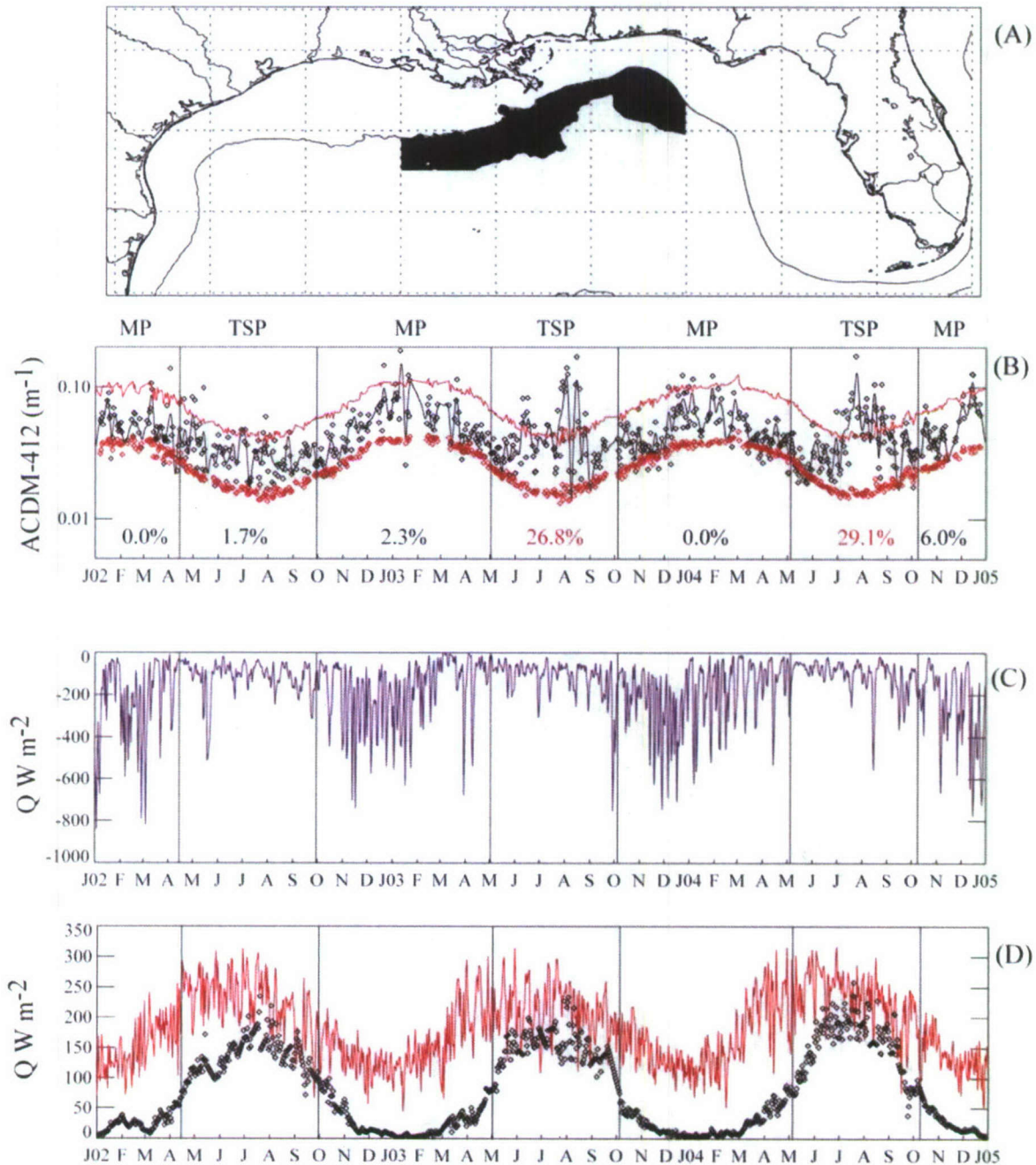
Figure 15. (a) Map of extracted area (shaded region 300–2000 m depth). (b) The time series of the mean CDM absorption values (at 412 nm) from the shaded area is shown as black triangles; the solid black line corresponds to the low-pass filtered values. The mean of the CDM absorption values hindcast by the empirical bio-thermal model are also shown (red triangles; Figure 15b). The red dashed line corresponds to the positive anomaly criterion (thermal hindcast value +100% log-space error). The percentages of low-pass filtered SeaWiFS-estimated values that exceed this positive anomaly criterion for each thermal period are shown; values exceeding 10% are shown in red. (c) The local NCEP reanalysis estimate of latent heat flux. (d) The NCEP shortwave heat flux component is shown as the red line; the average MODAS-estimated STR-30 values are also shown (black triangles; STR-30 × 2000).

thesis) within the surface mixed layer. In terms of the shortwave irradiant contribution to net heat flux, however, it is not sufficiently intense during winter to prohibit net losses of thermal energy from the surface ocean. Net heat losses promote vertical mixing, and hence the entrainment of dissolved inorganic nutrients required for primary productivity. The result is a characteristically subtropical winter peak in surface chlorophyll concentrations across the Gulf.

Thus the seasonal variation of solar insolation strikes contrasting balances between other apparently unrelated physical and biological processes that nonetheless act in concert to produce the observed bio-optical property distributions.

[58] The consistently negative correlation identified between satellite estimates of surface CDM absorption coefficients and upper ocean thermal energy further implies that photochemical processes other than photosynthesis may also warrant consideration. Whereas the vast majority of shortwave irradiance absorbed in the surface ocean is lost as heat, a small fraction may indeed stimulate abiotic photochemical reactions that tend to remove or photobleach the colored portion of nonliving organic materials. Assuming that the rate of photochemical degradation is proportional to the shortwave irradiant intensity, the thermal consequences of a vernal increase in solar insolation may reinforce and exacerbate the photochemical consequences. There are two main elements to this coupled process to consider: (1) shortwave irradiant intensity is attenuated with increasing depth, such that the nonliving organic matter nearer the surface is subjected to a greater potential for photochemical degradation whilst the increasing thermal energy creates density gradients that restrict these materials to near-surface layers; and (2) replenishment of the surface bio-optical signal would presumably depend upon the mixing of materials from depth, be they dissolved nutrients to stimulate near-surface primary productivity or additional colored dissolved materials produced within the deep ocean. Indeed, such replenishment likely occurs during the winter as the shortwave irradiant intensity declines, the frequency of latent heat loss events increases, the surface ocean begins to lose thermal energy, and the upper ocean density gradients are consequently reduced.

[59] Taken together, these mechanistic hypotheses imply that as the thermal energy of a parcel of water within the euphotic zone increases, both inorganic nutrients and CDM absorption are progressively depleted: the multifaceted consequences of shortwave irradiance absorption in the surface ocean. Accordingly, it is not surprising that the mesoscale circulation appears to enhance the inverse relationship between CDM absorption and upper ocean thermal energy: convergent, warm-core (divergent, cold-core) centers of circulation appear to result in below (above) average surface CDM absorption values. Presuming the gain in thermal energy for a near-surface water parcel is accompanied by a photochemically stimulated loss of CDM absorption, convergent circulation centers may tend to accumulate low-CDM absorption, high-thermal energy water parcels that, in turn, depress isotherms and greatly diminish the opportunity for near-surface CDM replenishment. Conversely, divergent circulation centers provide for such a replenishment scenario due to the uplift of isotherms (and by inference material property isopleths) towards the center of circulation. Indeed, an empirical bio-thermal model that accounts for both the seasonal bio-thermal cycle and the mesoscale modulation of it may explain roughly half of the variance in the satellite CDM absorption estimates. Some of the remaining variance appears to be associated with episodic interaction of the circulation with the continental shelves.

[60] The results thus imply that there are at least three basic scales of coupled biological-physical interactions impacting the biogeochemical processes of the surface ocean overlying the deep Gulf of Mexico: (1) the seasonal cycle of thermal stratification followed by winter overturn; (2) the mesoscale circulation of warm and cold-core eddies; and (3) the deep Gulf's interaction and water mass exchange with the continental shelves. Having established this basic construct for coupled bio-thermal observations, important questions remain as to the quantitative importance of these processes to the overall biogeochemistry of the Gulf. For example, interaction of mesoscale eddies with the shelf, as shown in Figure 13, may result in important local areas of high primary production [Biggs and Muller-Karger, 1994]; how do these local events impact the overall productivity of the deep Gulf? Conversely, interaction of the deep Gulf's circulation with the shelves may initiate a sequence of events that have biogeochemical consequences for coastal regions [Weisberg and He, 2003; Walsh et al., 2003]. Furthermore, these types of interactions may potentially be impacted by interannual variability in the duration of the thermally stratified or mixing periods. Understanding how these three scales interact to impact the biogeochemistry of the entire Gulf is an important avenue of future research.

Appendix A: Ocean Color Algorithm Validation

[61] The QAA was validated with in situ data by Lee et al. [2002] and again in the International Ocean-Colour Coordinating Group's Fifth Report [IOCCG, 2006]. The initial validation of the QAA was made by comparing the QAA-derived absorption coefficients with in situ measurements [Lee et al., 2002]. The majority of the in situ data used for this exercise did, in fact, come from the Gulf of Mexico, including stations in the deep Gulf, the West Florida Shelf, and near the Mississippi River Delta [see Lee et al., 1998]. In the second round of algorithm validation, the QAA was applied to the SeaBASS data set [Werdell and Bailey, 2005] wherein ~25% of the stations occupied were in the Gulf of Mexico. The QAA estimate of CDM absorption (at 443 nm) had a RMSE (root-mean-square error in log scale) of 0.221 when compared to the in situ observations (n = 630). When compared to a synthetic data set calculated by the radiative transfer simulation Hydrolight [Mobley, 1994], the QAA performed, as expected, even better (RMSE = 0.093). These results suggest that the inversion procedure used to decompose remotely sensed reflectance into constituent absorption coefficients is well-formulated.

[62] The OC4v4 chlorophyll is more widely used within the ocean color community and has been extensively tested [Bailey and Werdell, 2006; McClain et al., 2006]. When compared against the deep-water entries in the SeaBASS data set, the OC4v4 algorithm had an RMSE of 0.406 and a mean percent error of ±25.96 % (n = 271) [Bailey and Werdell, 2006]. Indeed, all of the above mentioned ocean color algorithms work best in oceanic waters [Lee et al., 2002; Bailey and Werdell, 2006]. Since our analysis avoids coastal regions where sediment suspension, bottom reflectance, and other coastal complexities may impede accurate product retrieval, we are more confident in these satellite estimates of surface bio-optical properties.

[63] Nevertheless, since our analysis also relies heavily upon general spatiotemporal trends observed in the satellite ocean color products, we performed an additional correla-

tion analysis between the SeaWiFS-based estimates of chlorophyll-*a*, phytoplankton absorption, and CDM absorption and the corresponding Gulf of Mexico in situ observations of these quantities within the NOMAD data set [*Werdell and Bailey*, 2005]. The satellite image pixel nearest the corresponding in situ record of latitude and longitude was selected for the satellite/in situ comparison, and the linear correlation coefficient (r) was calculated for the log-transformed values. The combined chlorophyll/absorption entries in the NOMAD data set are exclusively from the Ecology and Oceanography of Harmful Algal Blooms (ECOHAB) study of the West Florida Shelf wherein the average water depth was ~31-m. Despite the additional complexities of coastal waters, the satellite estimates of chlorophyll (r = 0.93), phytoplankton absorption (r = 0.89), and CDM absorption (r = 0.85) were all significantly correlated ($P < 0.0005$) to the in situ observations (n = 82). We are thus confident that this analysis of general trends in a large set of deep-water satellite estimates (n = 14,958,405) reasonably reflects the general trends that would arise from a similar analysis of ~15 million in situ observations.

Appendix B: Postprocessing Procedure for Ocean Color Data

[64] A consistent source of error in ocean color data arises from optical sensor ringing; the radiometer is unable to adjust to large contrasts in brightness near the edges of bright targets, such as the surface of a cloud [*Mueller*, 1988; *Yeh et al.*, 1997]. The result is an irregular pattern of very high product values near the edges of clouds. This is sometimes referred to in the literature as image speckling [*Uz and Yoder*, 2004]. To correct for this potential source of error in these data, an algorithm was developed to examine pixels near bright source targets based on the methods proposed by *Yeh et al.* [1997] and *Muller-Karger et al.* [1991]. Any pixel adjacent to a bright target (identified during processing as cloud, stray light, or high sun glint) was deleted, and any pixel within 14 pixel counts of a bright target was compared to all adjacent valid range pixels with respect to the remotely sensed reflectance contrast in the 510 nm band. If the absolute reflectance difference exceeded 0.0034 sr^{-1} then both pixels were deleted. This procedure likely eliminated valid pixels; however, this loss of data must be weighed against the effective removal of significant image speckling.

[65] The remaining product values were log-transformed and the mean, *m*, and variance, s^2, of the log-transformed values were calculated to determine the maximum likelihood estimator (MLE) within each regular interval 1/32 degree grid cell:

$$MLE = \exp\left(m + 0.5s^2\right) \tag{B1}$$

This method is preferable to the arithmetic mean since the probability density function of radiance values and derivative products approximates a lognormal distribution [*Campbell*, 1995]. All radiance-based bio-optical means referred to in the results were calculated according to

equation (B1). Moreover, the standard deviation for bio-optical products was computed as:

$$SD = \sqrt{\exp[2m + 2s^2] - \exp[2m + s^2]} \tag{B2}$$

The standard error was computed as equation (B2) divided by the total number of elements within the data array.

References

Agawin, N. S. R., C. M. Duarte, and S. Augustí (2000), Nutrient and temperature control of the contribution of picoplankton to phytoplankton biomass and production, *Limnol. Oceanogr.*, *45*, 591–600.

Amon, R. M. W., and R. Benner (1996), Photochemical and microbial consumption of dissolved organic carbon and dissolved oxygen in the Amazon River system, *Geochem. Cosmochim. Acta*, *60*, 1783–1792.

Andrews, S. S., S. Caron, and O. C. Zafiriou (2000), Photochemical oxygen consumption in marine waters: a major sink for colored dissolved organic matter?, *Limnol. Oceanogr.*, *45*, 267–277.

Bailey, S. W., and P. J. Werdell (2006), A multi-sensor approach for the on-orbitvalidation of ocean color satellite data products, *Remote Sens. Environ.*, *102*, 12–23.

Bidigare, R. R., M. E. Ondrusek, and J. M. Brooks (1993), Influence of the Orinoco River outflow on distributions of algal pigments in the Caribbean Sea, *J. Geophys. Res.*, *98*, 2259–2269.

Biggs, D. C., and F. E. Muller-Karger (1994), Ship and satellite observations of chlorophyll stocks in interacting cyclone-anticyclone eddy pairs in the western Gulf of Mexico, *J. Geophys. Res.*, *99*, 7371–7384.

Biggs, D. C., and P. H. Ressler (2001), Distribution and abundance of phytoplankton, zooplankton, ichthyoplankton, and micronekton in the deepwater Gulf of Mexico, *Gulf Mexico Sci.*, *1*, 7–29.

Bretherton, F. P., R. E. Davis, and C. B. Fandry (1976), A technique for objective analysis and design of oceanographic experiments applied to MODE-73, *Deep Sea Res.*, *23*, 559–582.

Bricaud, A., M. Babin, A. Morel, and H. Claustre (1995), Variability in the chlorophyll-specific absorption coefficients of natural phytoplankton: Analysis and parameterization, *J. Geophys. Res.*, *100*, 13,321–13,332.

Bricaud, A., E. Bosc, and D. Antoine (2002), Algal biomass and sea surface temperature in the Mediterranean Basin: Intercomparison of data from various satellite sensors, and implications for primary production, *Remote Sens. Environ.*, *81*, 163–178.

Bricaud, A., H. Claustre, J. Ras, and K. Oubelkheir (2004), Natural variability of phytoplankton absorption in oceanic waters: Influence of the size structure of algal populations, *J. Geophys. Res.*, *109*, C11010, doi:10.1029/2004JC002419.

Campbell, J. W. (1995), The lognormal distribution as a model for bio-optical variability in the sea, *J. Geophys. Res.*, *100*, 13,237–13,254.

Carder, K. L., R. G. Steward, G. R. Harvey, and P. B. Ortner (1989), Marine humic and fulvic acids: their affects on remote sensing of ocean chlorophyll, *Limnol. Oceanogr.*, *34*, 68–81.

Carder, K. L., S. K. Hawes, K. A. Baker, R. C. Smith, R. G. Steward, and B. G. Mitchell (1991), Reflectance model for quantifying chlorophyll-*a* in the presence of productivity degradation products, *J. Geophys. Res.*, *96*, 20,599–20,611.

Carder, K. L., F. R. Chen, Z. P. Lee, S. K. Hawes, and D. Kamykowski (1999), Semianalytic Moderate-Resolution Imaging Spectrometer algorithms for chlorophyll a and absorption with Bio-optical domains based on nitrate depletion temperatures, *J. Geophys. Res.*, *104*, 5403–5421.

Chassignet, E. P., H. E. Hurlburt, O. M. Smedstad, C. N. Barron, D. S. Ko, R. C. Rhodes, J. F. Shriver, A. J. Wallcraft, and R. A. Arnone (2005), Assessment of data assimilative ocean models in the Gulf of Mexico

using ocean color, in *Circulation of the Gulf of Mexico: Observations and Models*, edited by W. Sturgis and A. Lugo-Fenandez, pp. 87–100, AGU, Washington, D. C.

Chen, R. F., and J. L. Bada (1992), The fluorescence of dissolved organic matter in seawater, *Mar. Chem.*, *37*, 191–221.

Chen, R. F., W. P. Bissett, P. G. Coble, R. Conmy, G. B. Gardner, M. A. Moran, X. Wang, M. L. Wells, P. Whelan, and R. G. Zepp (2004), Chromophoric dissolved organic matter (CDOM) source characterization in the Louisiana Bight, *Mar. Chem.*, *89*, 257–272.

Chisholm, S. W. (1992), Phytoplankton size, in *Primary Productivity and Biogeochemical Cycles in the Sea*, edited by P. G. Falkowski and A. D. Woodhead, pp. 213–237, Plenum, New York.

Claustre, H. (1994), The trophic status of various oceanic provinces as revealed by phytoplankton pigment signatures, *Limnol. Oceanogr.*, *39*, 1206–1210.

Claustre, H., A. Bricaud, M. Babin, F. Bruyant, L. Guillou, F. Le Gall, D. Marie, and F. Partensky (2002), Diel variations in Prochlorococcus optical properties, *Limnol. Oceanogr.*, *47*, 1637–1647.

Cleveland, J. S. (1995), Regional models for phytoplankton absorption as a function of chlorophyll-*a* concentration, *J. Geophys. Res.*, *100*, 13,333–13,344.

Coble, P. G., C. E. Del Castillo, and B. Avril (1998), Distribution and optical properties of CDOM in the Arabian Sea during the 1995 Southwest Monsoon, *Deep Sea Res., Part II*, *45*, 2195–2223.

Dagg, M. J. (1988), Physical and biological responses to the passage of a winter storm in the coastal and inner shelf waters of the northern Gulf of Mexico, *Cont. Shelf Res.*, *8*, 167–178.

Del Castillo, C. E., F. Gilbes, P. G. Coble, and F. E. Muller-Karger (2000), On the dispersal of riverine colored dissolved organic matter over the West Florida Shelf, *Limnol. Oceanogr.*, *45*, 1425–1432.

Del Castillo, C. E., P. G. Coble, R. N. Conmy, F. E. Müller-Karger, L. Vanderbloemen, and G. A. Vargo (2001), Multispectral in situ measurements of organic matter and chlorophyll fluorescence in seawater: Documenting the intrusion of the Mississippi River plume in the West Florida Shelf, *Limnol. Oceanogr.*, *46*, 1836–1843.

Del Vecchio, R., and N. V. Blough (2002), Photobleaching of chromophoric dissolved organic matter, *Mar. Chem.*, *78*, 231–253.

Devred, E., S. Sathyendranath, V. Stuart, H. Maass, O. Ulloa, and T. Platt (2006), A two-component model of phytoplankton absorption in the open ocean: Theory and application, *J. Geophys. Res.*, *111*, C03011, doi:10.1029/2005JC002880.

DiMego, G. J., L. F. Bosart, and G. W. Endersen (1976), An examination of the frequency and mean conditions surrounding frontal incursions into the Gulf of Mexico and Caribbean Sea, *Mon. Weather Rev.*, *104*, 709–718.

Dowgiallo, M. J. (1994), Coastal oceanographic effects of the 1993 Mississippi river flooding, 76 pp., NOAA Coastal Ocean Off./Natl. Weather Serv., Silver Spring, Md.

Dunn, D. D. (1996), Trends in nutrient inflows to the Gulf of Mexico from streams draining the conterminous United States, 1972–93, *U.S. Geol. Surv. Water Resour. Invest. Rep.*, *96-4113*.

Elliot, B. A. (1982), Anti-cyclonic rings in the Gulf of Mexico, *J. Phys. Oceanogr.*, *12*, 1292–1309.

Espinosa-Carreon, T. L., P. T. Strub, E. Breier, F. Ocampo-Torres, and G. Gaxiola-Castro (2004), Seasonal and interannual variability of satellite-derived chlorophyll pigment, surface height, and temperature off Baja California, *J. Geophys. Res.*, *109*, C03039, doi:10.1029/2003JC002105.

Estrada, M., C. Marrase, and M. Alcarez (1988), Phytoplankton response to intermittent stirring and nutrient addition in marine microcosms, *Mar. Ecol. Prog. Ser.*, *48*, 225–234.

Falkowski, P. (1994), The role of phytoplankton photosynthesis in global biogeochemical cycles, *Photosyn. Res.*, *39*, 235–258.

Fox, D. N., C. N. Barron, M. R. Carnes, M. Booda, G. Peggion, and J. Van Gurley (2002a), The Modular Ocean Data Assimilation System, *Oceanography*, *15*, 22–28.

Fox, D. N., W. J. Teague, C. N. Barron, M. R. Carnes, and C. M. Lee (2002b), The Modular Ocean Data Assimilation System (MODAS), *J. Atmos. Oceanic Technol.*, *19*, 240–252.

Geider, R. J. (1987), Light and temperature dependence of the carbon to chlorophyll ratio in microalgae and cyanobacteria: Implications for physiology and growth of phytoplankton, *New Phytol.*, *106*, 1–34.

Gilbes, F., C. Tomas, J. J. Walsh, and F. E. Muller-Karger (1996), An episodic chlorophyll plume on the West Florida Shelf, *Cont. Shelf Res.*, *16*, 1201–1224.

Gilbes, F., F. E. Muller-Karger, and C. E. Del Castillo (2002), New evidence for the West Florida Shelf Plume, *Cont. Shelf Res.*, *22*, 2479–2496.

Gill, A. E. (1982), *Atmosphere-Ocean Dynamics*, 662 pp., Academic, New York.

Goolsby, D. A., W. A. Battaglin, B. T. Aulenbach, and R. P. Hooper (2001), Nitrogen input to the Gulf of Mexico, *J. Environ. Qual.*, *30*, 329–336.

Green, S. A., and N. V. Blough (1994), Optical absorption and fluorescence properties of chromophoric dissolved organic matter in natural waters, *Limnol. Oceanogr.*, *39*, 1903–1926.

Harris, G. (1986), *Phytoplankton Ecology: Structure, Function, and Fluctuation*, 384 pp., Springer, New York.

Harvey, G. R., D. A. Boran, L. A. Chesal, and J. M. Tokar (1983), The structure of marine humic and fulvic acids, *Mar. Chem.*, *12*, 119–132.

Hedges, J. I., R. G. Keil, and R. Benner (1997), What happens to terrestrial organic matter in the ocean?, *Org. Geochem.*, *27*, 195–212.

Hepplewhite, C. L. (1989), Remote observation of the sea surface and atmosphere: the oceanic skin effect, *Int. J. Remote Sens.*, *10*, 801–810.

Hochman, H. T., J. J. Walsh, K. L. Carder, A. Sournia, and F. E. Muller-Karger (1995), Analysis of ocean color components within stratified and well-mixed waters of the English Channel, *J. Geophys. Res.*, *100*, 10,777–10,787.

Hu, C., F. E. Muller-Karger, D. C. Biggs, K. L. Carder, B. Nababan, D. Nadeau, and J. Vanderbloemen (2003), Comparison of ship and satellite bio-optical measurements on the continental margin of the NE Gulf of Mexico, *Int. J. Remote Sens.*, *24*, 2597–2612.

Huh, O. K., W. J. Wiseman Jr., and L. J. Rouse Jr. (1978), Winter cycle of sea surface thermal patterns, northeastern Gulf of Mexico, *J. Geophys. Res.*, *83*, 4523–4529.

International Ocean-Colour Coordinating Group (IOCCG) (2006), Remote sensing of inherent optical properties: Fundamentals, tests of algorithms, and applications, edited by Z.-P. Lee, *Rep. 5*, Dartmouth, Canada. (Available at http://www.ioccg.org)

Jochens, A. E., S. F. DiMarco, W. D. Nowlin Jr., R. O. Reid, and M. C. Kennicutt II (2002), Northeastern Gulf of Mexico Chemical Oceanography and Hydrography Study, synthesis report, 586 pp., U.S. Dep. of the Inter., Minerals Manage. Serv., Gulf of Mexico OCS Region, New Orleans, La.

Jolliff, J. K., et al. (2003), Dispersal of the Suwannee River plume over the West Florida Shelf: Simulation and observation of the optical and biochemical consequences of a flushing event, *Geophys. Res. Lett.*, *30*(13), 1709, doi:10.1029/2003GL016964.

Kamykowski, D., and S. J. Zentara (2003), Can phytoplankton community structure be inferred from satellite-derived sea surface temperature anomalies calculated relative to nitrate depletion temperatures?, *Remote Sens. Environ.*, *86*, 444–457.

Kara, A. B., P. A. Rochford, and H. E. Hurlburt (2000), Mixed layer depth variability and barrier layer formation over the North Pacific Ocean, *J. Geophys. Res.*, *105*, 16,783–16,801.

Kieber, D. J. (2000), Photochemical production of biological substrates, in *The Effects of UV Radiation in the Marine Environment*, edited by S. J. de Mora et al., pp. 131–148, Cambridge Univ. Press, New York.

Kieber, R. J., X. Zhou, and K. Mopper (1990), Formation of carbonyl compounds from UV-induced photodegradation of humic substances in natural waters: Fate of riverine carbon in the sea, *Limnol. Oceanogr.*, *35*, 1503–1515.

Kirk, J. T. O. (1994), *Light and Photosynthesis in Aquatic Ecosystems*, 509 pp., Cambridge University Press, Cambridge.

Kudryavstev, V. N., and A. V. Soloviev (1989), Slippery near-surface layer of the ocean arising from daytime solar heating, *J. Phys. Oceanogr.*, *20*, 617–628.

Lambert, C. D., T. S. Bianchi, and P. H. Santschi (1999), Cross-shelf changes in phytoplankton community composition in the Gulf of Mexico (Texas shelf/slope): the use of plant pigments as biomarkers, *Cont. Shelf Res.*, *19*, 1–21.

Leben, R. R., and G. H. Born (1993), Tracking loop current eddies with satellite altimetry, *Adv. Space Res.*, *13*, 325–333.

Lee, Z., K. L. Carder, and R. A. Arnone (2002), Deriving inherent optical properties from water color: a multiband quasi-analytic algorithm for optically deep waters, *Appl. Opt.*, *41*, 5755–5772.

Lee, Z. P., K. L. Carder, R. G. Steward, T. G. Peacock, C. O. Davis, and J. S. Patch (1998), An empirical algorithm for light absorption by ocean water based on color, *J. Geophys. Res.*, *103*, 27,967–27,978.

Lentz, S. J. (2001), The influence of stratification on the wind-driven cross-shelf circulation over the North Carolina Shelf, *J. Phys. Oceanogr.*, *31*, 2749–2760.

Lewis, J. K., and A. D. Kirwan (1985), Some observations of ring topography and ring-ring interactions in the Gulf of Mexico, *J. Geophys. Res.*, *90*, 9017–9028.

Li, W. K. W. (2002), Macroecological patterns of phytoplankton in the northwestern North Atlantic Ocean, *Nature*, *419*, 154–157.

Longhurst, A. R. (1995), Seasonal cycles of pelagic production and consumption, *Prog. Oceanogr.*, *36*, 77–167.

MacIntyre, H. L., T. M. Kana, T. Anning, and R. J. Geider (2002), Photoacclimation of photosynthesis irradiance response curves and photosynthetic pigments in microalgae and cyanobacteria, *J. Phycol.*, *38*, 17–38.

Mann, K. H., and J. R. N. Lazier (1996), *Dynamics of Marine Ecosystems: Biological-Physical Interactions in the Oceans*, 2nd ed., 394 pp., Blackwell Sci., Cambridge, Mass.

Marañón, E., P. M. Holligan, R. Barciela, N. Gonzalez, B. Mourino, M. J. Pazo, and R. Varela (2001), Patterns of phytoplankton size structure and productivity in contrasting open-ocean environments, *Mar. Ecol. Prog. Ser.*, *216*, 43–56.

Maritorena, S., D. A. Siegel, and A. R. Peterson (2002), Optimal tuning of a semi-analytic model for global applications, *Appl. Opt.*, *41*, 2705–2714.

Martinolich, P. M. (2005), Automated processing system user's guide, version 3.0, internal publication, Nav. Res. Lab., Stennis Space Cent., Miss. (Available at http://www7333.nrlssc.navy.mil/docs/aps_v3.4/user/aps/)

Maul, G. A. (1977), The annual cycle of the Loop Current 1: Observations during a one-year time series, *J. Mar. Res.*, *35*, 29–47.

Maul, G. A., and H. R. Gordon (1975), On the use of the Earth Resources Technology Satellite (Landsat-1) in optical oceanography, *Remote Sens. Environ.*, *4*, 95–128.

Maul, G. A., and F. M. Vukovich (1993), The relationship between variations in the Gulf of Mexico Loop Current and Straits of Florida Volume Transport, *J. Phys. Oceanogr.*, *23*, 785–796.

McClain, C., S. Hooker, G. Feldman, and P. Bontempi (2006), Satellite data for ocean biology, biogeochemistry, and climate research, *Eos Trans. AGU*, *87*(34), 337.

Melo González, N., F. E. Muller-Karger, S. Cerdeira Estrada, R. Pérez de los Reyes, I. V. del Río, P. C. Pérez, and I. Mitrani Arenal (2000), Near-surface phytoplankton distribution in the western Intra-Americas Sea: The influence of El Niño and weather events, *J. Geophys. Res.*, *105*, 14,029–14,043.

Michaels, A. F., and D. A. Siegel (1996), Quantification of nonalgal light attenuation in the Sargasso Sea: Implications for biogeochemistry and remote sensing, *Deep Sea Res., Part II*, *43*, 321–345.

Millán-Núñez, E., M. E. Sieracki, R. Millán-Núñez, J. R. Lara-Lara, G. Gaxiola-Castro, and C. C. Trees (2004), Specific absorption coefficient and phytoplankton biomass in the southern region of the California Current, *Deep Sea Res., Part II*, *51*, 817–826.

Miller, W. L., and R. G. Zepp (1995), Photochemical production of dissolved inorganic carbon from terrestrial organic matter: significance to the oceanic carbon cycle, *Geophys. Res. Lett.*, *22*, 417–420.

Milliman, J. D., and R. H. Meade (1983), World-wide delivery of river sediment to the ocean, *J. Geol.*, *91*(1), 1–21.

Mobley, C. D. (1994), *Light and Water*, 595 pp., Academic, San Diego, Calif.

Mopper, K., and D. J. Kieber (2000), Marine photochemistry and its impact on carbon cycling, in *The Effects of UV Radiation in the Marine Environment*, edited by S. De Mora, S. Demers, and M. Vernet, pp. 101–129, Cambridge Univ. Press, Cambridge, Mass.

Mopper, K., Z. Xianliang, R. J. Keiber, D. J. Kieber, R. J. Sikorski, and R. D. Jones (1991), Photochemical degradation of dissolved organic carbon and its impact on the oceanic carbon cycle, *Nature*, *353*, 60–62.

Moran, M. A., and R. G. Zepp (1997), Role of photoreactions in the formation of biologically labile compounds from dissolved organic matter, *Limnol. Oceanogr.*, *42*, 1307–1316.

Morel, A., and A. Bricaud (1981), Theoretical results concerning light absorption in a discrete medium, and application to specific absorption of phytoplankton, *Deep Sea Res.*, *28*, 1375–1393.

Morell, J. M., and J. E. Corredor (2001), Photomineralization of fluorescent dissolved organic matter in the Orinoco River Plume: Estimation of ammonium release, *J. Geophys. Res.*, *106*, 16,807–16,813.

Morey, S. L., W. W. Schroeder, J. J. O'Brien, and J. Zavala-Hidalgo (2003), The annual cycle of riverine influence in the eastern Gulf of Mexico basin, *Geophys. Res. Lett.*, *30*(16), 1867, doi:10.1029/2003GL017348.

Morrison, J. M., and W. D. J. Nowlin (1976), Repeated nutrient, oxygen, and density sections through the Loop Current, *J. Mar. Res.*, *35*, 105–128.

Mueller, J. L. (1988), Nimbus-7 CZCS: Electronic overshoot due to cloud reflectance, *Appl. Opt.*, *27*, 438–440.

Mueller, J. L. (2000), SeaWiFS algorithm for the diffuse attenuation coefficient K(490): Using water-leaving radiances at 490 and 555 nm, *NASA Tech. Memo.*, *2000-206892*, *11*, 24–27.

Muller-Karger, F. E. (2000), The spring 1998 Northeastern Gulf of Mexico (NEGOM) cold water event: Remote sensing evidence for upwelling and eastward advection of Mississippi water (or: How an errant loop current anticyclone took the NEGOM for a spin), *Gulf Mexico Sci.*, *18*, 55–67.

Muller-Karger, F. E., C. McClain, T. R. Fisher, W. E. Esias, and R. Varela (1989), Pigment distribution in the Caribbean Sea: Observations from space, *Prog. Oceanogr.*, *23*, 33–64.

Muller-Karger, F. E., J. J. Walsh, R. H. Evans, and M. B. Meyers (1991), On the seasonal phytoplankton concentration and sea surface temperature

cycles of the Gulf of Mexico as determined by satellites, *J. Geophys. Res.*, *96*, 12,645–12,665.

Nelson, N. B., D. A. Siegel, and A. F. Michaels (1998), Seasonal dynamics of colored dissolved material in the Sargasso Sea, *Deep Sea Res., Part I*, *45*, 931–957.

Nelson, N. B., C. A. Carlson, and D. K. Steinberg (2004), Production of chromophoric dissolved organic matter by Sargasso Sea microbes, *Mar. Chem.*, *89*, 273–287.

Nelson, N. B., D. A. Siegel, C. A. Carlson, C. Swan, W. M. Smethie Jr., and S. Khatiwala (2007), Hydrography of chromophoric dissolved organic matter in the North Atlantic, *Deep Sea Res., Part I*, *54*, 710–731.

Obata, A., J. Ishizaka, and M. Endoh (1996), Global verification of critical depth theory for phytoplankton bloom with climatological in situ temperature and satellite ocean color data, *J. Geophys. Res.*, *101*, 20,657–20,667.

O'Reilly, J. E., et al. (2000), Ocean color chlorophyll-*a* algorithms for SeaWiFS, OC2 and OC4: Version 4, *NASA Tech. Memo.*, *2000-206892*, *11*, 9–23.

Qian, Y., A. E. Jochens, M. C. Kennicutt II, and D. C. Biggs (2003), Spatial and temporal variability of phytoplankton biomass and community structure over the continental margin of the northeast Gulf of Mexico based on pigment analysis, *Cont. Shelf Res.*, *23*, 1–17.

Rochelle-Newall, E. J., and T. R. Fisher (2002), Production of chromophoric dissolved organic matter fluorescence in marine and estuarine environments: an investigation into the role of phytoplankton, *Mar. Chem.*, *77*, 7–21.

Rodriguez, J., J. Tintore, J. T. Allen, J. M. Blanco, D. Gomis, A. Reul, J. Ruiz, V. Rodriguez, F. Echevarria, and F. Jiminez-Gomez (2001), Mesoscale vertical motion and the size structure of phytoplankton in the ocean, *Nature*, *410*, 360–363.

Sakshaug, E., K. Andresen, and D. A. Kiefer (1989), A steady state description of growth and light absorption in the marine planktonic diatom Skeletonema costatum, *Limnol. Oceanogr.*, *34*, 198–205.

Salisbury, J. E., J. W. Campbell, E. Linder, L. D. Meeker, F. E. Muller-Karger, and C. J. Vorosmarty (2004), On the seasonal correlation of surface particle fields with wind stress and Mississippi discharge in the northern Gulf of Mexico, *Deep Sea Res., Part II*, *51*, 1187–1203.

Sambrotto, R. N., H. J. Niebauer, J. J. Goering, and R. L. Iverson (1986), Relationships among vertical mixing, nitrate uptake, and phytoplankton growth during the spring bloom in the Southeast Bering Sea middle shelf, *Cont. Shelf Res.*, *5*, 161–198.

Sathyendranath, S., L. Watts, E. Devred, T. Platt, C. Caverhill, and H. Maass (2004), Discrimination of diatoms from other phytoplankton using ocean-colour data, *Mar. Ecol. Prog. Ser.*, *272*, 59–68.

Savidge, D. K. (2002), Wintertime shoreward near-surface currents south of Cape Hatteras, *J. Geophys. Res.*, *107*(C11), 3205, doi:10.1029/2001JC001193.

Schluessel, P., H.-Y. Shin, W. J. Emery, and H. Grassl (1987), Comparison of satellite-derived surface temperature with in situ skin measurement, *J. Geophys. Res.*, *92*(C3), 2859–2874.

Siegel, D. A., S. C. Doney, and J. A. Yoder (2002a), The North Atlantic spring phytoplankton bloom and Sverdrup's critical depth hypothesis, *Science*, *296*, 730–733.

Siegel, D. A., S. Maritorena, N. B. Nelson, D. A. Hansell, and M. Lorenzi-Kayser (2002b), Global distribution and dynamics of colored dissolved and detrital organic materials, *J. Geophys. Res.*, *107*(C12), 3228, doi:10.1029/2001JC000965.

Siegel, D. A., S. Maritorena, and N. B. Nelson (2005), Independence and interdependencies among global ocean color properties: Reassessing the bio-optical assumption, *J. Geophys. Res.*, *110*, C07011, doi:10.1029/2004JC002527.

Simeon, J., C. S. Roesler, W. S. Pegau, and C. Dupuoy (2003), Sources of spatial variability in light absorbing components along an equatorial transect from 165°E to 150°W, *J. Geophys. Res.*, *108*(C10), 3333, doi:10.1029/2002JC001613.

Smetacek, V., and U. Passow (1990), Spring bloom initiation and Sverdrup's critical depth model, *Limnol. Oceanogr.*, *35*, 228–234.

Sturges, W., and R. Leben (2000), Frequency of ring separations from the Loop Current in the Gulf of Mexico, *J. Phys. Oceanogr.*, *30*, 1814–1819.

Sverdrup, H. U. (1953), On conditions for the vernal blooming of phytoplankton, *J. Cons. Int. Explor. Mer*, *18*, 287–295.

Toner, M., A. D. Kirwan Jr., A. C. Pope, L. H. Kantha, F. E. Muller-Karger, and R. T. Jones (2003), Chlorophyll dispersal by eddy-eddy interactions in the Gulf of Mexico, *J. Geophys. Res.*, *108*(C4), 3105, doi:10.1029/2002JC001499.

Uz, B. M., and J. A. Yoder (2004), High frequency and mesoscale variability in SeaWiFS chlorophyll imagery and its relation to other remotely sensed oceanographic variables, *Deep Sea Res., Part II*, *51*, 1001–1017.

Valiela, I. (1995), *Marine Ecological Processes*, 2nd ed., 686 pp., Springer, New York.

Van der Leeden, F., F. L. Troise, and D. K. Dodd (1990), *The Water Encyclopedia*, 2nd ed., 824 pp., CRC Press, Boca Raton, Fla.

Virmani, J. I., and R. H. Weisberg (2003), Features of the observed annual ocean-atmosphere flux variability on the West Florida Shelf, *J. Clim.*, *16*, 734–745.

Vodacek, A., N. V. Blough, M. D. DeGrandpre, E. T. Peltzer, and R. K. Nelson (1997), Seasonal variation of CDOM and DOC in the Middle Atlantic Bight: Terrestrial inputs and photooxidation, *Limnol. Oceanogr.*, *42*, 674–688.

Vukovich, F. M. (1995), An updated evaluation of the Loop Currents eddy-shedding frequency, *J. Geophys. Res.*, *100*, 8655–8659.

Vukovich, F. M., and B. W. Crissman (1986), Aspects of warm rings in the Gulf of Mexico, *J. Geophys. Res.*, *91*, 2645–2660.

Walker, N. D. (1994), Satellite-based assessment of the Mississippi River discharge plume's spatial structure and temporal variability, OCS study MMS 94-0053, 56 pp., U.S. Dep. of the Inter., Minerals Manage. Serv., Gulf of Mexico OCS Region, New Orleans, La.

Walker, N. D. (1996), Satellite assessment of Mississippi Plume variability: causes and predictability, *Remote Sens. Environ.*, *58*, 21–35.

Walsh, J. J., D. A. Dieterle, M. B. Meyers, and F. E. Müller-Karger (1989), Nitrogen exchange at the continental margin: A numerical study of the Gulf of Mexico, *Prog. Oceanogr.*, *23*, 245–301.

Walsh, J. J., et al. (2003), Phytoplankton response to intrusions of slope water on the West Florida shelf: Models and observations, *J. Geophys. Res.*, *108*(C6), 3190, doi:10.1029/2002JC001406.

Weisberg, R. H., and R. He (2003), Local and deep-ocean forcing contributions to anomalous water properties on the West Florida Shelf, *J. Geophys. Res.*, *108*(C6), 3184, doi:10.1029/2002JC001407.

Werdell, P. J., and S. W. Bailey (2005), An improved in-situ bio-optical data set for ocean color algorithm development and satellite data product validation, *Remote Sens. Environ.*, *98*, 122–140.

Whitehead, R. F., S. J. de Mora, and S. Demers (2000), Enhanced UV radiation – a new problem for the marine envirnment, in *The Effects of UV Radiation in the Marine Environment*, edited by S. J. de Mora et al., pp. 1–34, Cambridge Univ. Press, New York.

Willis, J. K., D. Roemmich, and B. Cornuelle (2004), Interannual variability in the upper ocean heat content, temperature, and thermosteric expansion on global scales, *J. Geophys. Res.*, *109*, C12036, doi:10.1029/2003JC002260.

Wilson, C., and V. J. Coles (2005), Global climatological relationships between satellite biological and physical observations and upper ocean properties, *J. Geophys. Res.*, *110*, C10001, doi:10.1029/2004JC002724.

Yeh, E., M. Darzi, and K. Lakshmi (1997), SeaWiFS stray light correction algorithm, *NASA Tech. Memo.*, *104566*, *41*, 24–33.

Zavala-Hidalgo, J., S. L. Morey, and J. J. O'Brien (2003), Seasonal circulation on the western shelf of the Gulf of Mexico using a high-resolution numerical model, *J. Geophys. Res.*, *108*(C12), 3389, doi:10.1029/2003JC001879.

Zentara, S. J., and D. Kamykowski (1977), Latitudinal relationships among temperature and selected plant nutrients along the west coast of North and South America, *J. Mar. Res.*, *35*, 321–337.

Zimmerman, R. A., and D. C. Biggs (1999), Patterns of distribution of sound-scattering zooplankton in warm-core and cold-core eddies in the Gulf of Mexico from a narrowband acoustic Doppler current profiler survey, *J. Geophys. Res.*, *104*, 5251–5262.

R. Arnone, R. Helber, J. K. Jolliff, J. C. Kindle, Z. Lee, B. Penta, C. D. Rowley, and I. Shulman, Naval Research Laboratory, Stennis Space Center, MS 39529, USA. (jason.jolliff@nrlssc.navy.mil)